Realia et naturalia

DISSERTATIONES
PHYSICAE
UNIVERSITATIS
TARTUENSIS
91

KAUPO VOORMANSIK

X-band synthetic aperture radar applications for environmental monitoring

DISSERTATIONES PHYSICAE UNIVERSITATIS TARTUENSIS
91

DISSERTATIONES PHYSICAE UNIVERSITATIS TARTUENSIS
91

KAUPO VOORMANSIK

X-band synthetic aperture radar applications for environmental monitoring

UNIVERSITY OF TARTU
PRESS
1632

This study was carried out at AS Regio, German Aerospace Center (DLR), University of Tartu and Tartu Observatory.

The dissertation was admitted on 10.01.2014 in partial fulfilment of the requirements for the degree of Doctor of Philosophy in Physics, and was allowed for defence by the Council of the Institute of Physics, University of Tartu.

Supervisors: DSc Mart Noorma, University of Tartu, Estonia
PhD Rein Rõõm, University of Tartu, Estonia

Opponents: PhD Liis Sipelgas, Tallinn University of Technology, Estonia
PhD Laurent Ferro-Famil, University of Rennes, France

Defence: February 14, 2014, at the University of Tartu

These studies were supported by European Social Fund's Doctoral Studies and Internationalisation Programme DoRa. Programme DoRa is carried out by Archimedes Foundation.

ISSN 1406–0647
ISBN 978–9949–32–483–5 (print)
ISBN 978–9949–32–484–2 (pdf)

University of Tartu Press
www.tyk.ee

CONTENTS

LIST OF ORIGINAL PUBLICATIONS

This thesis is based on the following publications (full texts included at the end of the thesis), which are referred to in the text by their Roman numerals. The papers are reprinted with the kind permission of the publishers.

I K. Voormansik, J. Praks, O. Antropov, J. Jagomägi and K. Zalite, "Flood Mapping With TerraSAR-X in Forested Regions in Estonia," *IEEE Journal of Selected Topics in Applied Earth Observations and Remote Sensing*, in print, 2013.

II K. Zalite, K. Voormansik, A. Olesk, M. Noorma and A. Reinart, "Effects of Inundated Vegetation on X-Band HH–VV Backscatter and Phase Difference," *IEEE Journal of Selected Topics in Applied Earth Observations and Remote Sensing,* in print, 2013.

III K. Voormansik, T. Jagdhuber, A. Olesk, I. Hajnsek and K. P. Papahtanassiou, "Towards a detection of grassland cutting practices with dual polarimetric TerraSAR-X data," *International Journal of Remote Sensing*, vol. 34, no. 22, pp. 8081–8103, 2013.

IV K. Voormansik, T. Jagdhuber, I. Hajnsek and K. P. Papathanassiou, "Improving Semi-natural Grassland Administration with TerraSAR-X," in *Proceedings of the 17th GeoCAP Annual Conference*, edited by: D. Fasbender, K. Taşdemir, Ph. Loudjani, V. Angileri, C. Lucau, P. Milenov, W. Devos, R. De Kok, S. Lemajic, A. Tarko and P. Pizziol, pp. 26–32, Tallinn, 2011.

AUTHOR'S CONTRIBUTION

The articles on which this thesis is based are the result of collective work and contain important contributions from all the co-authors. The author's contribution to the publications referred to by their Roman numbers is indicated as follows:

I Planning and organizing the campaign; design of the experiments; satellite data processing; conducting the field works; analysis of the data processing results; full text of the article.

II Proposing the experiment, planning and organising the satellite data takes campaign, reviewing the manuscript.

III Planning and organizing the campaign; design of the experiments; satellite data processing; analysis of the data processing results; theoretical explanation with modelling; full text of the article.

IV Planning and organizing the campaign; design of the experiments; satellite data processing; analysis of the data processing results; oral presentation at the conference; full text of the article.

ABBREVIATIONS

ALOS	Advanced Land Observation Satellite
ASAR	Advanced Synthetic Aperture Radar
C-band	4.0–8.0 GHz electromagnetic spectrum frequency range
DLR	Deutsches Zentrum für Luft- und Raumfahrt – *German Aerospace Center*
EM	electro magnetic
IEM	Integral Equation Method
FBS	Fine Beam Single Polarisation
HH	horizontal transmit, horizontal receive
HV	horizontal transmit, vertical receive
Ku-band	12.0–18.0 GHz electromagnetic spectrum frequency
L-band	1.0–2.0 GHz electromagnetic spectrum frequency range
LAI	leaf area index
MODIS	Moderate-Resolution Imaging Spectroradiometer
MSG	Meteosat Second Generation
NASA	National Aeronautics and Space Administration
NDVI	normalised differential vegetation index
NESZ	noise equivalent sigma zero
NIR	near infra-red spectral range
P-band	250–500 MHz electromagnetic spectrum frequency range
PALSAR	Phased Array type L-band Synthetic Aperture Radar
SAR	synthetic aperture radar
US	United States
VH	vertical transmit, horizontal receive
VIS	visible spectral range
VV	vertical transmit, vertical receive
WSM	Wide Swath Mode
X-band	8.0–12.0 GHz electromagnetic spectrum frequency range

1. INTRODUCTION

1.1. Background

Recent advances in science and technology have certainly opened up new possibilities, but at the same time they have increased mankind's responsibilities. Mankind's capabilities and concrete actions in re-shaping the environment on Earth can be seen to have greatly increased between the 1800s and the year 2000. The majority of the scientific community agrees that there is evidence of anthropogenic influence on climate change [1,2]. The increased frequency of extreme weather events like heavy rainfall or hurricane-induced floods has also been connected with human-induced climate change [1,3]. Global warming accelerates the global water cycle and this causes such severe weather events to occur more frequently [2,4]. Even if there is not 100% agreement on the extent of anthropogenic causes for global warming [5,6], people still possess enough energy and technology to alter the natural processes of the Earth like never before in man's recorded history. Therefore, it is especially important nowadays to monitor and understand the processes of the environment and climate here on Earth.

There are several possibilities for monitoring and measuring the environment on Earth, e.g., by direct observations or using automated sensor networks. Earth observation satellites allow the monitoring of huge areas in a very short time and with a high refresh rate. The Meteosat Second Generation (MSG) satellite is the best example of high refresh rate huge area monitoring as it is able to collect data on more than 1/3 of the entire Earth's surface in the visible (VIS) and near infrared (NIR) spectral range with a 15 min refresh rate and a spatial resolution of 1–3 km [7]. In medium 250 m resolution, NASA MODIS instruments on the Aqua and Terra satellites can measure the reflected VIS and NIR sunlight from the entirety of the Earth's surface once every 24 hours [8]. Thus Earth observation satellites are established information sources for monitoring the environment on a regional and global scale. According to different sources, there are approximately 119–122 operational Earth observation satellites in orbit as of December 2013 [9,10].

Optical instruments mounted on Earth observation satellites have provided meteorological and environmental information since the launches of Vanguard 2 and Landsat-1 in 1959 and 1972 respectively [11,12]. Aside from the optical instruments' strengths in classifying different objects and materials using high spectral resolution imaging, there are also some major disadvantages. Optical instruments are dependent on sunlight – very limited information can be retrieved from night-time imaging and in the event of cloud cover the measurements rather contain information on the atmosphere but not the underlying land. Radar instruments can overcome both such limitations. As they carry their own source of illumination, radars are independent of sunlight. In addition, the microwave frequencies used in radars can penetrate the atmosphere in almost any weather conditions. It is thus possible to retrieve information about land

both during the day and at night, independently of cloud cover. In addition, imaging radars are sensitive to the electrical and structural properties of the sensed objects: they penetrate the canopy and returning echoes contain information about the entire vegetative structure depending on the plants' moisture content, not only about the upper layer reflectivity of vegetation like in passive optical remote sensing [13,14]. Radar remote sensing is vital in areas that are under almost constant cloud cover (like some equatorial regions or Northern Europe during autumn). Thanks to this canopy penetration, it is possible to measure forest structure and biomass as well as processes that take place under the forest canopy, like floods [13–15]. It is for these reasons that radars are considered to be more suitable than – or as complementary sensors to – optical remote sensing instruments in several applications.

Radars have been used to track ships and aircraft for almost a hundred years [13]. However, constructing a feasible imaging radar has been challenging. A simple real aperture radar installed on a satellite would need a very large antenna ($d>30$ m) with a very narrow beamwidth ($\theta<0.5°$) and still the resolution on the ground would be several kilometres in size, which is only suitable for very coarse wide-scale process monitoring. In the early 1950s C. A. Wiley and C. W. Sherwin *et al.* independently of each other suggested using the Doppler history of the signal to improve ground resolution much below the actual beamwidth [16,17]. Practical uses of high resolution Synthetic Aperture Radar (SAR) were, however, limited for some decades due to the extensive processing power needed for image focusing. In addition to SAR developments in military aircraft, the first successfully realised civilian space-borne SAR was NASA's Seasat in 1978 [18]. Although Seasat operated for only 106 days, it clearly demonstrated what microwave imaging radars were capable of and opened up the following era to their development.

After the theoretical work in SAR polarimetry carried out by Wolfgang-Martin Börner [19], NASA's AIRSAR sensor, first flown in 1987, demonstrated the value of polarimetric radar imaging for environmental monitoring [20]. The use of different polarisations can enhance the information content of imaging radar measurements [13,15]. Taking the structural properties of the sensed object, the recorded signal depends on the polarisation of the incident and received electromagnetic waves [13,15]. Hence, using different polarisations allows the retrieval of detailed information about the sensed object structure and acquisition geometry.

SAR and polarimetric SAR can be used for acquiring timely information about natural disasters to make better informed decisions for mitigating their effects. Floods are one of the most common disasters, occurring more often because of the accelerated water cycle due to global warming [2,4], causing 142 billion US dollars of damage and affecting almost 1 billion people for the past decade 2001–2010 [21]. Some years after the launch of Seasat in 1978 it was noticed that SAR images can reveal flooded areas due to enhanced backscatter in forested areas and reduced backscatter in open areas [22–25]. Models for flooded forest backscatter showed that the enhanced backscatter is most

likely caused by changes in the Fresnel power reflection coefficients [26] for the double bounce backscattering mechanism [27] when there is standing water under forest canopy. For flood mapping in the forest, longer wavelengths like those in the L-band [27–29], steep incidence angles (20°–30°) [27–31] and HH (Horizontal transmit, Horizontal receive) polarization [28,32,33] are shown to be well suited to this purpose due to the high contrast between flooded and non-flooded forest. For shallower incidence angles the radar beam must travel a longer distance through canopy, thus attenuating more [27,30]. Shorter wavelengths like those in the C- and X-band attenuate more in the canopy [27,29]. Other polarisations like VV (Vertical transmit, Vertical receive) and HV (Horizontal transmit, Vertical receive) interact more with the canopy, thus backscattering more from branches and leaves and less from the ground [28,34]. C-band SAR, however, is also shown to be suitable for flood detection under the forest canopy; it has demonstrated up to 98% classification accuracy in leaf-off conditions [35], and in leaf-on conditions this accuracy is reduced (89%) [35,36]. Besides simple backscatter threshold methods [37,38], the exploitation of complex coherence information [39–42] is proven feasible for flood mapping in open areas. On this relatively mature physical basis, the focus of the past seven years' research has been in creating a fully automatic SAR-based flood mapping algorithm [43–46,21]. High population density urban areas and their rapid flood mapping for disaster relief are of special interest to the research community. Recent works by Mason *et al*. have demonstrated promising results when exploiting digital surface and building models to solve the radar shadow and layover effects and improve the results with modelling [47,48].

Grassland parameter retrieval is another SAR application with high potential. More than 40% of the Earth's surface is covered by various grasslands [49], therefore in the context of global warming and sustainable development it is important to trace the changes and understand the processes of such a widespread type of land cover. Also, from the perspective of the development of precision farming [50,51], grassland information retrieval is needed to minimise maintenance costs while reducing the ecological footprint of farming. Here, again, imaging radars are the preferred sensors primarily because of their weather independence [13]. With imaging radars it is possible to set up a regular and continuous time series of measurements to follow the whole phenological cycle of a field.

In the case of grasslands, the recorded SAR signal is in general a mixture of volume scattering from grass plants and surface scattering from the soil [52]. When studying backscattered signal magnitude, low frequencies like L-band and HV polarisation are found to provide close to linear proportional correlation with high dynamic range (9–14 dB) to grass height and biomass [53,54]. In higher frequencies like C-band, the proportional dynamic range to grass height is lower (2–3 dB) [54,55]. Even higher frequencies like X- and Ku-band, an inverse relation to backscattered signal magnitude and grass-like plant height is found [56,57]. The backscattered signal from soil is mainly dependent on its moisture content [58–60], surface roughness [61,62], tillage practices [63,64]

and row orientation relative to the SAR flight path [63,65,66]. The choice of polarisation and incidence angle determines whether the radar echo corresponds more to soil or to vegetation scattering. It has been shown that shallow incidence angles (>40°) and VV or HV polarisation interact more with vegetation, with a smaller portion of energy being backscattered from the soil [67,68]. HV polarised measurements are also shown to be almost independent of different row orientations relative to the sensor's flight path [63,69,70]. Vegetation response to microwaves could be successfully modelled by a cloud of dipoles and spheres where the predicted SAR signal is strongly dependent on the orientation of the dipoles [14]. Model predictions [14] are in line with real observations where wind-induced leaf tilt and grain lodging altered the SAR signal by 5–7 dB [56,57].

The recent launches of X-band SAR satellites TerraSAR-X [71] and COSMO SkyMED [72] in 2007 have opened up new possibilities for SAR-based applications development. Not only is the spatial resolution of 1 m [73,74] unprecedented, but also X-band SAR scattering properties have not been very closely studied so far and the limits of such systems are not yet fully understood. For flood mapping, high resolution X-band SAR theoretically allows the production of very accurate flood maps. For grassland parameter retrieval, the polarimetric modes of TerraSAR-X could potentially provide information about the vegetation's structure and moisture in fine resolution.

1.2. Objectives and progress in this work

The usability of short wave X-band SAR for flood mapping in temperate forest was studied. The experiments performed at the Estonian Alam-Pedja Nature Reserve in April 2010 proved that X-band SAR can penetrate the canopy enough to reveal standing water under coniferous and leaf-off deciduous forests **[I, II]**. The experiment, supported by field measurements, reveals large enough differences in backscatter levels to distinguish flooded areas from non-flooded areas in deciduous leaf-off, coniferous and mixed forests. Before the studies carried out for this thesis, it was commonly believed that X-band SAR energy is backscattered from treetops and is thus not suitable for flood detection in forest areas [27–29]. Within the study **[I],** the first high-resolution satellite remote sensing-based flood maps of the Alam-Pedja Nature Reserve were also produced. The Alam-Pedja Nature Reserve is a rich ecosystem that finds itself regularly flooded and the flood maps are a basis for further ecological studies of this area.

In this thesis the performance of X-band SAR's HH-VV polarimetric channel for flooded forest detection was measured for the first time. From the SAR polarimetry models, enhanced backscatter in flooded forest is known to correspond to the double bounce mechanism in the HH-VV polarimetric channel [13]. Therefore the backscatter difference between flooded and non-flooded forest should be higher in HH-VV than in the HH polarimetric channel.

In order to measure the improvement in using the X-band SAR HH-VV polarimetric channel, an experiment was conducted in a North European temperate forest **[II]**. The LIDAR-aided experiment demonstrated an improvement of 0.2–1.6 dB in the HH-VV channel over conventional HH in flooded vs. non-flooded forest backscatter-based distinction. Another indicator of forest flooding is a phase shift towards 180° between the HH and VV polarimetric channels. In this experiment **[II]** a phase difference change of around 60° to 70–87° was measured. These results are useful for applying polarimetric X-band SAR data for flood detection in temperate forest areas.

The first detection of grass cutting with dual polarimetric HH/VV X-band SAR was tested **[III, IV]**. The first experiments at the Matsalu test-site in 2011 with dual polarimetric HH/VV TerraSAR-X measurements gave a partial solution. One specific behaviour in the dominant scattering alpha angle was found to indicate the areas where grass had been cut and was left lying on the ground. However, no reliable difference in the dual polarimetric HH/VV TerraSAR-X observables was found when comparing tall grass fields with short grass fields whose grass had already been collected. The random volume over ground backscattering model for vegetation scattering [14] was applied and the changes in alpha scattering angle were well explained when tall grass was cut and left lying on the ground **[III, IV]**.

2. FLOOD DETECTION WITH X-BAND SAR IN NORTHERN EUROPEAN TEMPERATE FORESTS [Publications I and II]

2.1. Physical basis for microwave scattering

Microwave scattering can be fully described using Maxwell's equations for electromagnetic (EM) wave propagation, the electrical and structural properties of the sensed object and the medium [75–77]. Propagation through a medium and the scattering from an object is determined by its relative permittivity [77]. Relative permittivity is a complex-valued parameter where the real part represents capacitance and the imaginary part attenuation. The greater the capacitance the greater the amount of incident electromagnetic energy is reflected from the surface, and the less is therefore refracted into the object. The greater the imaginary part of relative permittivity the faster the electromagnetic energy will attenuate in a given medium. Relative permittivity is a function of the frequency of EM waves, e.g., for water in the most common spaceborne SAR frequency range of 1–10 GHz the relative permittivity changes from 80+6i to 63+30i [78], see Figure 2.1. For natural sites, the most prominent changes in microwave scattering occur because of changes in water content and distribution, as water is one of the most variable parameters in the atmosphere, biosphere and lithosphere and its relative permittivity is high compared to other natural materials like air, wood and sand. The relative permittivity of air is close to 1 [77], for dry wood it ranges from 2+0.05i to 4+0.15i [79], for dry sand from 2+0.015i to 3+0.01i [80] and for dry ice up to about 3+0.01i [81].

In addition to this frequency-dependent relative permittivity, the dimensions of the sensed objects are also important. The waves interact only with objects of the same dimension or bigger than the given wavelength [13,14]. Therefore, longer wavelengths like 23 cm in L-band almost do not interact with tree leaves at all (even if their moisture content is high) and most of the energy is backscattered from branches, tree-trunks and the ground in the case of backscattering in the forest [15].

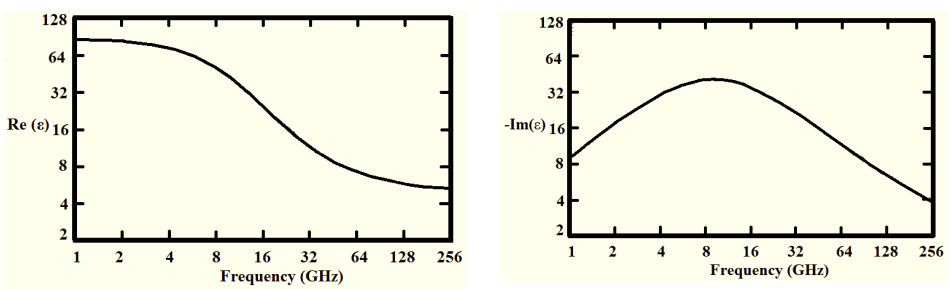

Figure 2.1. Relative permittivity (ε) of water for frequencies 1–256 GHz. Left diagram represents the real and right side the imaginary part, according to [78].

Thanks to microwave EM radiation's strong interaction with liquid water, various SAR applications like soil moisture retrieval, snow classification and flood mapping are possible [13–15].

2.2. Scattering mechanisms in flooded forest

The scattering mechanisms for a forest scene are presented in Figure 2.2. The SAR-measured backscatter σ^0 is composed of backscattered radiation from the canopy (σ^0_c), tree trunks (σ^0_t), surface (σ^0_s), double bounce from the trunk and surface (σ^0_d) and other multipath (e.g., triple bounce) backscattering (σ^0_m). The composition of the measured backscatter σ^0 is described by Equation (1), where a_c is the attenuation in canopy and trunk. All values in Equation (1) are in linear scale.

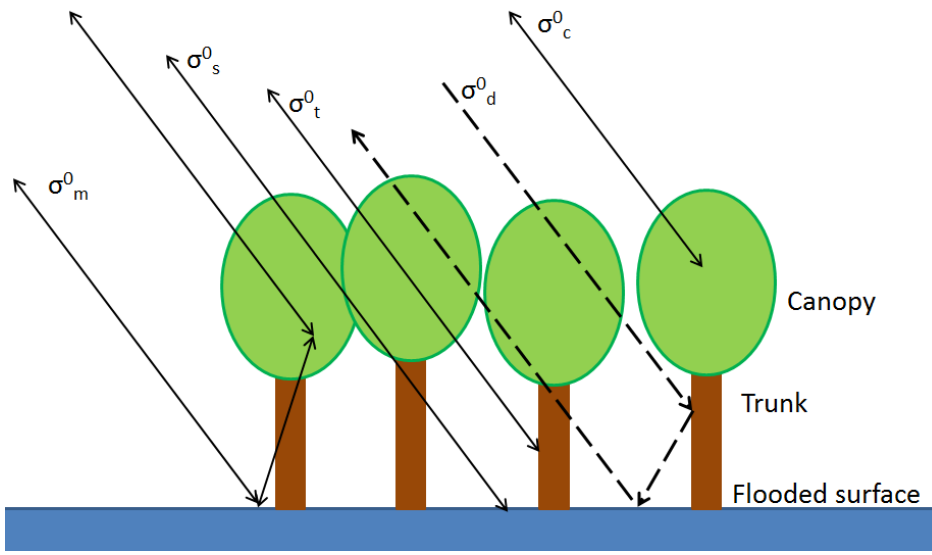

Figure 2.2. Scattering mechanisms in flooded forest, backscattering from the trunk (σ^0_t), surface (σ^0_s), double-bounce from the trunk and surface (σ^0_d), multipath back-scattering (σ^0_m) and canopy (σ^0_c).

$$\sigma^0 = \sigma_c^0 + a_c{}^2(\sigma_m^0 + \sigma_t^0 + \sigma_s^0 + \sigma_d^0) \quad (1)$$

It is interesting to note that the double bounce mechanism directs the incident SAR pulse energy almost exactly back to the sensor independently from the incident angle. The angle between a tree trunk and the surface is close to 90°, acting like a corner reflector. Comparing flooded and unflooded conditions, backscatter coefficients from the surface (σ^0_s) and the double bounce (σ^0_d)

change significantly and cause overall registered backscatter change up to 10 dB [82]. In flooded conditions the surface backscattering coefficient (σ^0_s) is usually lower, except in the case of windy weather when the water's surface is rougher thanks to the waves and backscatter from the surface is thereby increased. With a smooth water surface, specular reflection directs most of the energy away from the sensor, whereas for unflooded conditions the rougher forest ground causes a greater amount of radar energy to be scattered backwards, resulting in higher σ^0_s [27]. For similar reasons, during flooding the double bounce coefficient (σ^0_d) is enhanced since the forward scattering efficiency factor is much higher due to the smooth water surface [27].

The canopy and trunk attenuation coefficient a_c is a function of radar frequency. For higher frequencies like 9.65 GHz in X-band the attenuation is greater (lower a_c) than 1.27 GHz in L-band. There are two main reasons for the attenuation coefficient's frequency dependence. Firstly, canopy and trunks contain water and the EM waves' loss factor (imaginary part of relative permittivity) increases when frequencies increase from 1 to 10 GHz (see Figure 2.1 for details). Secondly, for higher frequencies the radar pulses interact more with the leaves and branches as there are more objects with dimensions of 3 cm and larger (X-band) than there are objects measuring 23 cm and larger (L-band) [27].

Because of the higher frequencies' greater attenuation in canopy and trunks, lower frequencies like in L-band are generally preferred for flood mapping in forests [29]. However, there are practical considerations due to the limitations of spectrum allocation. For remote sensing purposes more bandwidth is available in X-band than in L-band. As SAR image range resolution is directly proportional to bandwidth [83], higher resolution imaging is possible in X-band than in L-band. Thus X-band SAR would allow the generation of high-resolution forest flood maps – something which was not possible before with L-band systems – when canopy and trunk penetration is sufficient.

2.3. Flooded area detection based on enhanced backscatter

In spring 2010, a flood mapping campaign at the Alam-Pedja Nature Reserve in Estonia was arranged with TerraSAR-X in order to test X-band SAR's ability to detect flooding under temperate forest. During the campaign there was a record flood in Alam-Pedja, the biggest in over 50 years, with a 330 cm water level maximum in the river Emajõgi [84] and over 210 km^2 of flooded area [**I**]. The test site is mainly covered with glades, deciduous, coniferous and mixed forests, and bogs. Tree height in the deciduous, coniferous and mixed forests where the X-band performance assessment was done was 15–25 m [85] at that time. The deciduous trees were in leaf-off conditions during the experiment in spring 2010.

A total of 5 TerraSAR-X images were used in the campaign: two *stripmap* HH polarisation images with a mean incidence angle of 24° and spatial

resolution of 3 m, acquired on 5 and 27 April; two *stripmap* HH polarisation images with a mean incidence angle of 43° and spatial resolution of 3 m, acquired on 6 and 28 April; and one *scanSAR* HH polarisation image with a mean incidence angle of 42° and spatial resolution of 18 m, acquired on 15 April. All the images were used for flood map creation and the X-band SAR performance assessment for forest flood mapping was based on the *scanSAR* image. The *scanSAR* image was selected because it captured the flood maximum (large flooded area and good selection of test forests) and there were other SAR acquisitions available for comparison at that time. An ENVISAT ASAR HH polarised 150 m resolution 24° incidence angle WSM image acquired on 14 April and an ALOS PALSAR HH polarised 12.5 m resolution 34.3° incidence angle FBS image acquired on 16 April were used for cross-validation. In the field surveys, the flooded areas were marked on maps that were later extended using ALOS PALSAR imagery since HH-polarised L-band SAR is a proven tool for flood detection in forests [23,24,27]. Additional details about the test site and data processing methodology are given in **Publication I**.

Based on the experiment, 6.2, 3.2 and 4.0 dB higher backscatter was registered in deciduous, mixed and coniferous forest when comparing flooded conditions with non-flooded. The backscatter enhancement proved sufficiently accurate for detailed flood map generation, as presented in **[I]**. The incidence angle in the test was 42°. According to the previous studies, steeper incidence angles should produce higher backscatter enhancements [27,36] and, for TerraSAR-X's steeper incidence angles of 20–30°, the flooded vs. non-flooded forest distinction is likely even higher. On the other hand, the experiment was carried out in April during leaf-off conditions and attenuation a_c is likely greater for summer leaf-on conditions, thus reducing backscatter enhancement due to flooding.

The fact that flooded areas were successfully detected under 15–25 m tall forest means that there was relatively deep forest penetration. The relatively deep forest penetration of X-band SAR pulses observed is in line with later TanDEM-X measurements in tropical forest [86]. The study [86] suggests an interesting explanation for the relatively deep forest penetration of X-band: on one hand the X-band microwaves are more attenuated in the canopy than L-band microwaves but, on the other hand, as the waves themselves are smaller in X-band than in L-band (3 cm vs 23 cm) it is more likely that the ground is reached through the small holes in the forest cover.

2.4. Improved flooded forest detection with HH-VV polarimetric channel

From ordinary single-channel polarisations such as HH, HV and VV, generally HH is preferred for flood mapping in forest thanks to greater ground contribution and less interaction with the canopy than for HV or VV channels [27,28,32, 33]. However, for multi-polarisation polarimetric radar measurements, new

polarimetric channels could be formed using the Pauli basis [13,87]. The complex HH+VV and HH-VV polarimetric channels are shown to correspond to odd bounce (e.g., single bounce from surface) and even bounce (e.g., a double bounce from water surface and tree-trunk) scattering respectively [14]. For ideal surface scattering the HH+VV channel is in the maximum and HH-VV is zero. For ideal double bounce scattering the HH-VV channel is in the maximum and the HH+VV channel is zero. Therefore, the HH-VV channel should be the most natural choice for high-contrast flooded forest detection.

The complex HH-VV polarimetric channel is in the maximum for the double bounce scattering mechanism due to the 180° phase jump after double bounce scattering. According to electromagnetic theory, the phase of horizontally polarised waves is flipped 180° after a single forward scattering from a perfectly conducting surface (Figure 2.3a), whereas for vertically polarised waves the phase remains unchanged after a single forward scattering from a perfectly conducting surface [88]. Hence the phase difference between HH and VV polarimetric channels is 180° after a double bounce scattering from a perfectly conducting dihedral.

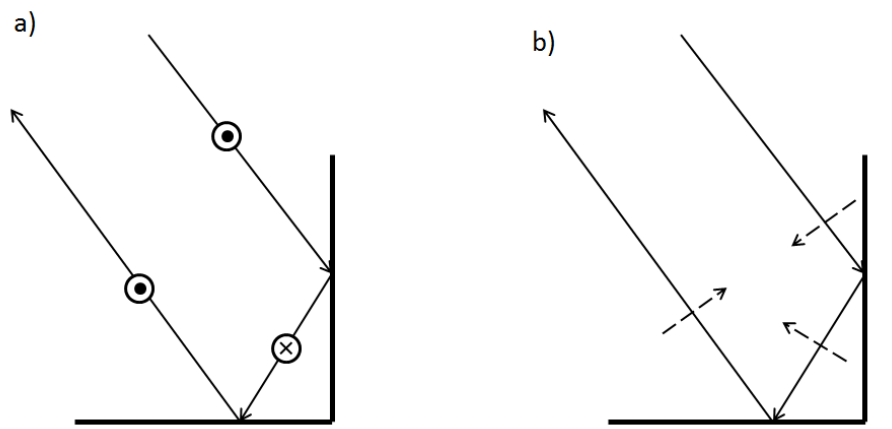

Figure 2.3. The phase changes of horizontally (a) and vertically (b) polarized EM waves during the double-bounce reflection from an ideal dihedral.

In order to test the improved flooded vs. non-flooded forest distinction of the HH-VV polarimetric channel over a conventional HH channel, an experiment was organised in Soomaa National Park, Estonia in spring 2012 using TerraSAR-X dual polarimetric HH/VV data. The stand corresponded to a typical Northern European temperate forest with forest cover of 75–81%. During the experiment the forests were in leaf-off conditions. The radar data was acquired with an incidence angle of 23°. Additional details of the experiment are presented in Publication **II**. Flooded forest conditions in Soomaa in March 2012 are shown in Figure 2.4.

Figure 2.4. Flooded deciduous forest in Soomaa during leaf-off conditions in late March 2012.

The measured improvement of HH-VV compared to the HH polarimetric channel in a flooded vs. non-flooded forest distinction was 0.2–1.6 dB, depending on forest type. The improvement of using HH-VV was greater in deciduous forest than in coniferous forest (see Figure 2.5 for details).

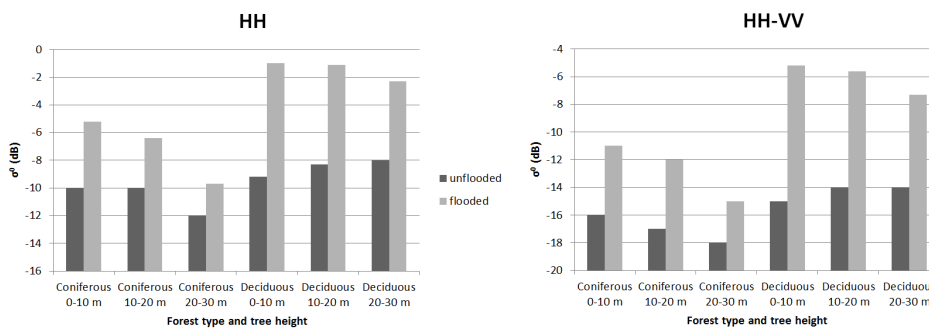

Figure 2.5. Backscatter coefficients (σ^0) in deciduous and coniferous forest for flooded and unflooded conditions, HH and HH-VV polarimetric channels.

2.5. Phase difference of HH and VV polarimetric channels

In order to better understand the greater flooded vs. non-flooded forest backscatter difference in the HH-VV channel, the polarimetric phase difference between HH and VV channels was examined within the same research study [**II**] for both flooded and non-flooded conditions. In addition, the polarimetric phase difference between HH and VV channels could itself be used as a parameter for the detection of flooded areas [89].

For double bounce scattering from tree trunks and the ground, the characteristic phase difference between HH and VV is 180°. For canopy single-bounce scattering the phase difference is likely close to 0°. In real forest conditions the overall phase difference between HH and VV falls within the range of 0–180° depending on forest conditions and radar frequency. For example, for C-band and coniferous forest in Howland, US, the recorded mean phase difference between HH and VV was 85° [90]. Overall, phase difference is greater for longer wavelengths like in P- and L-band and for sparser, smaller-canopy forest because of the greater double-bounce portions in the backscattered SAR energy.

The recorded phase differences for flooded and unflooded conditions in temperate forest in X-band according to the 2012 campaign are presented in Figure 2.6.

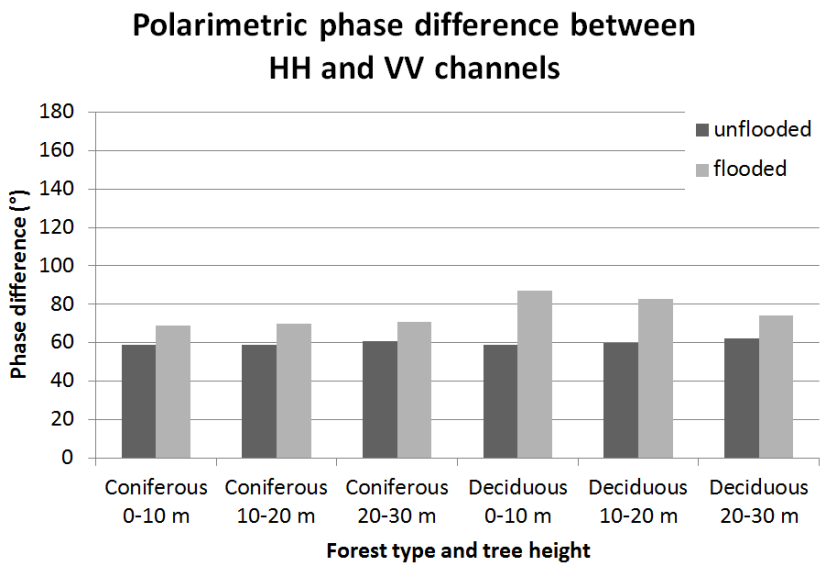

Figure 2.6. HH and VV channel polarimetric phase differences for deciduous and coniferous forest for flooded and unflooded conditions.

In non-flooded conditions the phase difference between HH and VV channels is close to 60° regardless of forest type (Figure 2.6). In flooded conditions the phase difference is not uniform in different types of forest. In coniferous forests the phase difference increases by about 10° regardless of forest height. In deciduous forest the greatest phase difference increase (28°) happens in forests with the lowest tree cover ranging from 0–10 m. The greatest phase difference increase also causes the biggest improvement (1.6 dB) when using the HH-VV channel instead of HH (see Figure 2.5).

The stand height-dependent phase difference in deciduous forest could be explained by the increased travel path though the canopy (forest cover was very similar for all stands – 75–81%). For taller forests travel through the canopy was longer and the attenuation was also greater, thus reducing the double bounce component as described by Equation (1).

The stand height-independent phase difference increase in coniferous forest is not so intuitive to understand. As cover in all three different forest height stands was similar (75–80%), the phase difference increase should be smaller for taller forests due to greater attenuation in the canopy and smaller double bounce contributions. However, this is not what is observed. One possible explanation for this behaviour might be connected to the developmental phases of the coniferous spruce and pine trees common on the Soomaa test site. For these spruce and pine trees, the height of the layer of living branches covered with needles is almost constant whether the tree height be 10 or 30 m. The lower part of the pine trees is almost bare trunk without any branches, and the lower part of a spruce tree in a relatively dense forest is covered only by some dead branches without needles. Therefore, the attenuating canopy layer could be almost of the same thickness for coniferous forests with different tree heights, resulting in similar double-bounce portions in the recorded SAR signal.

Above, the advantages of using dual polarimetric SAR measurements for forest flood mapping were demonstrated. Backscatter difference between flooded and non-flooded conditions is greater in the HH-VV channel compared to single channel HH data. It is also possible to exploit polarimetric phase changes between the HH and VV channels for the delineation of flooded areas [89]. However, for practical applications one also needs to consider the disadvantages of the dual polarimetric modes of SAR systems. Swath width and/or the resolution of dual polarimetric modes are usually inferior to those of the single channel mode of the same sensor. For TerraSAR-X the azimuth resolution is two times coarser and the swath width two times narrower in dual polarimetric mode compared to single channel *stripmap* mode [73]. ALOS PALSAR's dual polarimetric mode range resolution is two times coarser compared to its single channel mode [91].

2.6. Flood map generation

There are several methods for flood map generation based on SAR measurements: using backscatter enhancements, texture and coherence changes, being single image or time-series based [23,25,40,92,93]. Time-series generally give more accurate results, but in emergency situations usually just a single image is available and therefore the ability to delineate flooded areas from a single image is important [21]. In the study **[I],** flood map generation based on a single SAR acquisition was demonstrated.

Even when flooded forest could be separated from unflooded forest from studying its enhanced backscatter, accurate flood map generation may require additional information from other sources. In the 2010 campaign the wet fields resulted in very similar backscatter levels to those of flooded forest (see Figure 2.7) even when there was no open liquid water in the fields. In order to filter out the wet fields, a forest cover vector layer was used as described in Publication **I**.

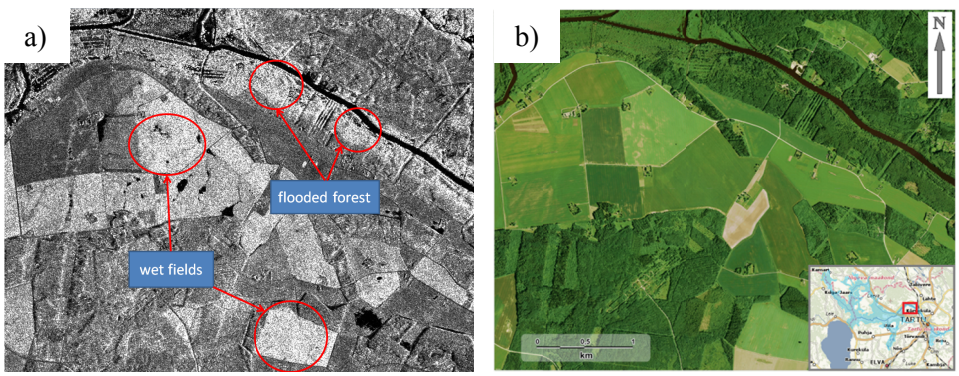

Figure 2.7. Wet fields and flooded forest in April 2010 near Emajõgi river produce very similar backscatter (a). Ortophoto of the same area (b) [94].

It is also important to take into account the inherent speckle effect of SAR images. Due to the random phase summation of backscattered waves, either constructive or destructive interference occurs within a resolution cell. Therefore, SAR images appear noisy even in homogeneous areas [13]. In **[I]** the Frost speckle suppression filter and a morphological opening and closing operator was used to generate a smooth flooded-area bitmap for vectorisation. Similar results might be achieved with the Refined Lee speckle filter [95] and the median filter for later binary flood map smoothing. Considering the median filter, it is necessary to run the filter through many iterations in order to achieve convergence and similar results to a single run of the morphological open/close operator.

Examples of the remote sensing-based flood maps are presented in Publication **I** figures 11 and 13.

3. DUAL POLARIMETRIC X-BAND SAR SIGNATURES OF GRASSLANDS [Publications III and IV]

There are several good reasons for grassland monitoring. It is one the most common land cover types, grasslands covering more than 40% of the Earth [49]. Following the changes in grasslands will help to understand changes in global ecology and the climate. In the European Union subsidies are paid to farmers proportionally to the area of grassland they possess and maintain on a yearly basis. Therefore, remote sensing-based grassland monitoring could avoid expensive and labour-intensive field work, thus saving the costs of validating subsidy claims. Finally, the retrieved grassland parameters would represent important input for precision farming applications [50,51].

It is possible to monitor grassland with optical remote sensing instruments in the visible and near infrared (NIR) spectral range [96]. Indexes derived from multispectral measurements, like the NDVI (Normalised Differential Vegetation Index) and LAI (Leaf Area Index), are sensitive to grass plants' chlorophyll content, and through the chlorophyll content a biomass estimation can be derived [97,98]. However, these well-established grassland monitoring optical methods only work with clear skies. Depending on geographical location, cloud cover can make regular optical grassland monitoring methodology unreliable.

Polarimetric SAR, being weather and sunlight independent, is an option for regular grassland monitoring. Unlike optical sensors, it is not sensitive to chlorophyll content but to the structural properties and water content of the grass plants and the soil [13–15].

The current study is one of the first to explore polarimetric X-band SAR capabilities for grassland parameter retrieval. Grasslands have been studied with polarimetric SAR at lower frequencies like in P-, L- and C-band [59,96], but there have been almost no grassland studies carried out using polarimetric X-band SAR.

The experiment was carried out close to Matsalu bay, Northern Europe, Estonia near the banks of the Kasari river in the summer of 2011. A total of 7 TerraSAR-X HH/VV acquisitions with a mean incidence angle of 36.9° were considered from June to October. All satellite data captures were supported by field surveys including grass height measurements and photographs to capture the actual conditions in the grass fields. Field survey, meteorological and satellite data details are given in Publications **III** and **IV**.

3.1. TerraSAR-X dual polarimetric HH/VV mode

TerraSAR-X dual polarimetric modes provide a reliable data source for regular weather-independent grassland monitoring. There are three options for the dual polarimetric mode polarisation choice: HH/VV, HH/HV and VV/VH [73]. While HV and VH (Vertical transmit, Horizontal receive) polarimetric channels are shown to be sensitive to the forest and herbaceous biomass due to volume scattering [99], it is not a preferred option for grassland parameter retrieval with TerraSAR-X. The Noise Equivalent Sigma Zero (NESZ) of TerraSAR-X is –19 dB and typical backscatter levels for X-band co-polarised channels (VV or HH) in grasslands are between –15 to –10 dB, but for cross-polarised channels (VH or HV) typical backscatter levels are –25 to –20 dB. The HV and VH channels lying under the noise level of the sensor makes using them very difficult.

Additionally, the phase difference between HH and VV channels for natural targets contains information, whereas the polarimetric phase difference between a cross-pol. channel (HV or VH) and a co-pol. channel (HH or VV) is completely random [13,14]. In TerraSAR-X dual polarimetric measurements, not only are the amplitudes of the two channels recorded but also the relative phase between the polarimetric channels. Hence HH/VV dual polarimetric mode provides three independent parameters for each natural target pixel, while HH/HV and VV/VH modes have only two – the amplitudes of the response. Different resolution and swath width dual polarimetric HH/VV modes are described in Table 3.1 below. Based on a calibration campaign, the polarimetric phase offset between the HH and VV channels was between +1° to –3° [100].

Table 3.1 TerraSAR-X dual polarimetric HH/VV modes [73].

	Stripmap	**Spotlight**	**High-resolution spotlight**
Resolution (ground range X azimuth)	3.5–1.9 m X 6.6 m	3.6–1.7 m X 3.4 m	3.6–1.7 m X 2.2 m
Field of view (ground range X azimuth)	15 km X 50 km	10 km X 10 km	10 km X 5 km
Recommended incidence angle range	19.9°–40.3°	19.7°–43.3°	19.7°–43.3°

3.2. Dual polarimetric entropy/alpha decomposition

For distributed natural targets, each resolution cell in a SAR image is composed of responses from different objects with different scattering mechanisms. The contributions from different scatterers are coherently added in random phase; this causes the recorded signal magnitude and phase to vary significantly even for homogeneous land cover. In order to overcome the spatial randomness of polarimetric SAR data, spatially averaged coherency or covariance matrixes could be formed [13,101]. To distinguish this different scattering mechanism from the covariance or coherency matrix data and describe the sensed objects, decomposition theorems could be applied. In the current experiment the coherency matrix [101] and eigenvalue/eigenvector-based entropy/alpha decomposition [102] are used. In order to be applicable for the TerraSAR-X HH/VV datasets, the dual pol. extension [103] using the T_{22} coherency matrix [104] is employed. The processing chain together with its exact parameters is explained step-by-step in Publication **III**.

3.3. Dual polarimetric signatures of grasslands

The parameters calculated from the TerraSAR-X dataset included dual polarimetric entropy, mean alpha scattering angle, dominant alpha scattering angle, coherence magnitude and phase between HH+VV and HH-VV polarimetric channels, coherence magnitude and phase between HH and VV polarimetric channels, |HH|/|VV| intensity ratio, HH, VV, HH+VV and HH-VV backscatter.

Grass height in the different fields ranged from 5 cm to 70 cm during the observed time period from June to October 2011. After analysing the above-mentioned dual polarimetric X-band SAR parameters, none of them was found to be sensitive to grass height. However, distinct signatures were found for grass that was cut and lying on the ground. One of the most prominent parameters indicating cut grass lying on the ground was the dominant alpha scattering angle. For growing grass (no matter whether the height was 5 or 70 cm) the dominant alpha scattering angle was found to be constantly around 10° and it only rose to over 25° when the grass was cut and left uncollected in the fields. See Figure 3.1 for the time series for dominant scattering alpha angle from 19 June to 24 August. The green region of Test Field 1 (TF1) on 2 August (Figure 3.1c) was documented to correspond to cut grass lying on the ground with a field survey, and by 24 August (Figure 3.1d) the grass had already been collected and the dominant scattering alpha angle fell back to around 10°. Earlier, on images from 19 June (Figure 3.1a) and 11 July (Figure 3.1b), the grass heights on TF1 were of 60 and 70 cm respectively.

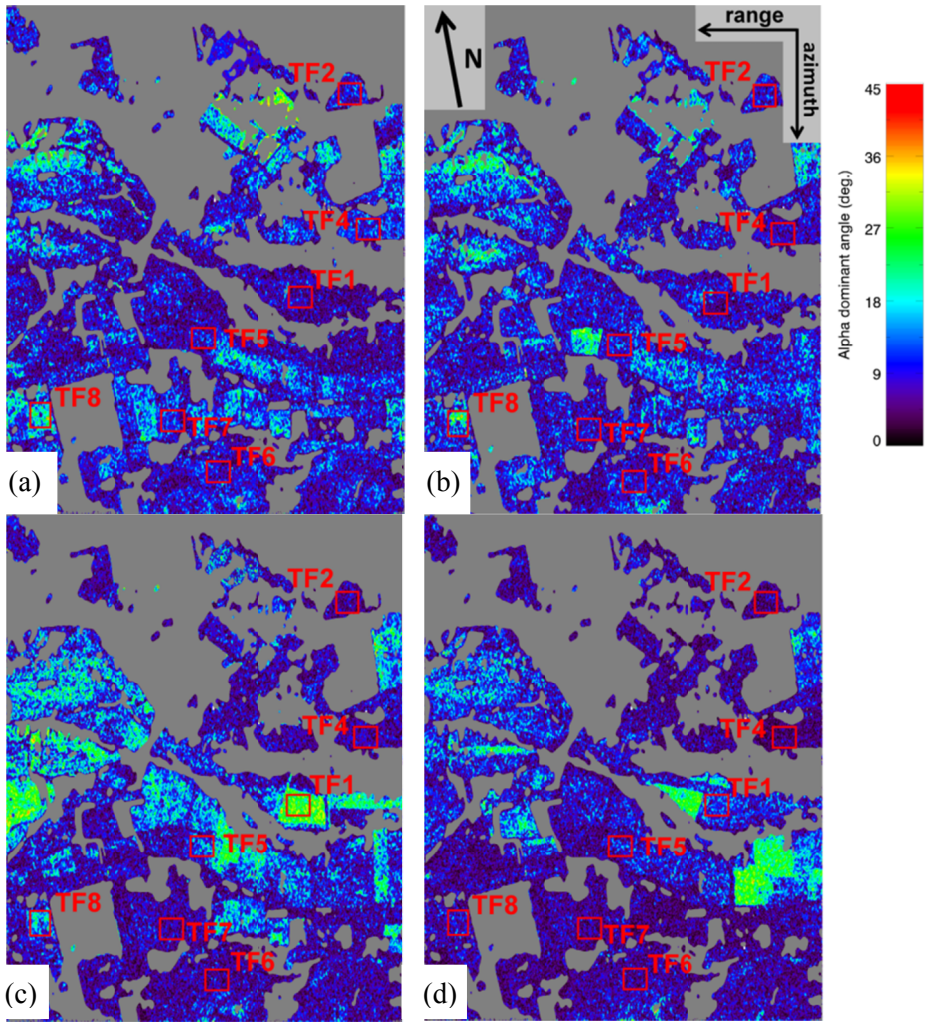

Figure 3.1. Dual polarimetric dominant alpha scattering angle in Matsalu test-fields on 19 June (a), 11 July (b), 2 August (c) and 24 August (d).

Other parameters sensitive to uncollected cut grass were the mean scattering alpha angle, T_{12} coherence (between HH+VV and HH-VV polarimetric channels) magnitude, HH/VV coherence phase and |HH|/|VV| intensity ratio (see Figure 3.2). In order to construct an algorithm for classifying the state of grassland, these parameters could be exploited.

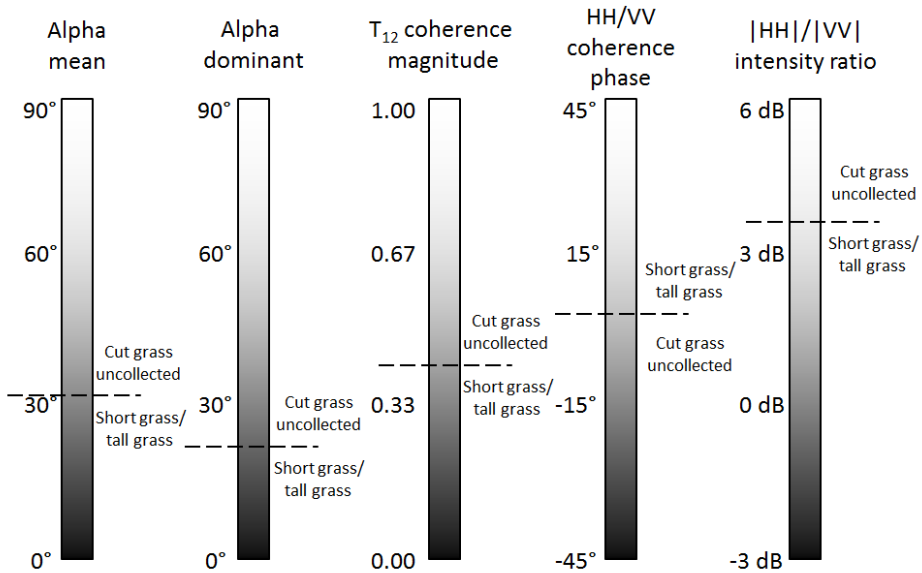

Figure 3.2. Polarimetric SAR parameters for detecting cut grass lying on the ground and the respective threshold values.

3.4. Wind and rain effects on grassland scattering

The SAR signal recorded over grassland is always a mixture of responses from the soil and the grass. Changing weather conditions can change the response from both soil and grass and, hence, also the relevant portions in the acquired signal. Recent rainfall prior to acquisition is likely to enhance backscattering from the grass because the relative permittivity of water is high (63+30i at 10 GHz) [78] and backscattering will happen more from the top grass layer and less from the underlying soil. Therefore the changes in the recorded SAR signal might also reflect the changes in grass plant water cover and not only in grass plant structure. The 2011 Matsalu campaign was, however, performed in relatively dry conditions: there was 0 mm of precipitation in the 24h-period prior to all satellite data captures from June to August, and only 0.2 and 4.6 mm for the 15 September and 7 October data captures respectively [105]. Hence, the trends observed from this study are likely to indicate changes in the grass and not in the water cover.

Similarly, the wind could affect the acquired SAR signal. Polarimetric SAR is sensitive to the structure and orientation of the sensed objects. Wind can change the orientation of the grass plants, thus changing the structure. A 7 dB increase in VV backscattering was observed in a barley field (similar plant structure to grass) when the wind bent the barley plants away from the side along which the SAR sensor was looking, compared to the case during still weather [56]. At the same time, backscattering in the HH channel also increased but at a lower magnitude of 2.5 dB [56]. This effect could be explained by

modelling the grass plants as vertically-oriented dipoles (see Figure 3.3). The response from a dipole is higher the better the alignment agrees with an EM wave's polarization. It is at its maximum, when the EM wave's oscillation is along the same plane as the dipole and when the direction of propagation is perpendicular to the dipole. SAR is a side-looking system with typical incidence angles of between 20°-45°. Then, for calm weather, the angle between the radar's line of sight (EM wave direction of propagation) and the grass plants acting as dipoles will also be between 20°–45° (Figure 3.3a). When the wind bends the grass plants away from the sensor, the angle between the radar's line of sight and the grass plants is closer to 90°, resulting in higher backscatter for vertically polarized EM waves (Figure 3.3b).

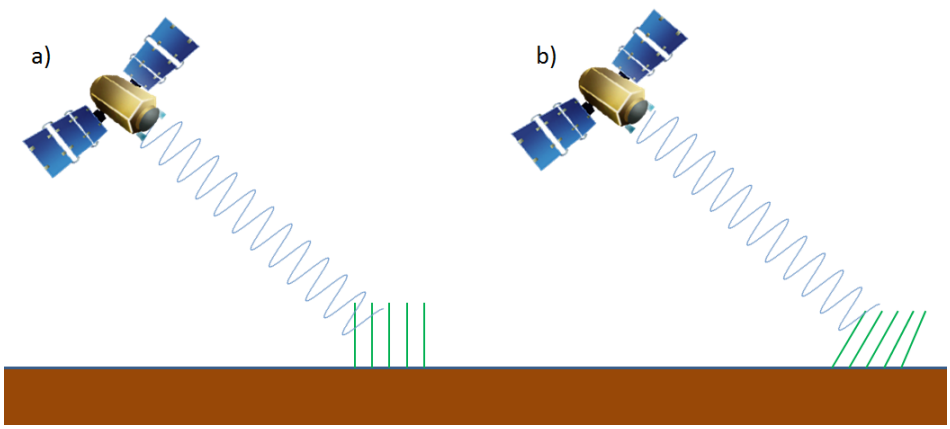

Figure 3.3. Grassland scattering geometry and vertically polarized EM waves in calm weather conditions (a) and with wind blowing in the same direction as the sensor's line of sight (b).

During the summer months June to August of the 2011 Matsalu campaign when the most prominent changes occurred in the grass fields (e.g., the dominant scattering alpha angle behaviour in Figure 3.1), there was almost calm weather. Wind speed at the closest meteorological station in Lääne-Nigula was measured at 0–3 m/s during the TerraSAR-X data captures from June to August [106]. It is therefore unlikely that wind-induced orientation effects significantly affected the results and conclusions of the Matsalu 2011 study.

3.5. Possible effects of soil moisture on grassland scattering

In section 3.3 it was described how a specific behaviour in the dual polarimetric SAR parameters was observed for cut grass lying on the ground. In order to distinguish changes in grassland structure and the water content of the plants from changes in the soil it is important to understand how changes in soil moisture would change observed SAR parameters. Moisture changes are the single most important factor altering the response from soil, when no ploughing has occurred like in the 2011 Matsalu campaign.

One possible explanation for the observed changes in the dominant alpha scattering angle is connected with changes in soil moisture. It was confirmed that no heavy rainfall had occurred at that time (0 mm precipitation 24h prior to the satellite data captures from June to August [105]), but it could have been the case that the uncollected cut grass accumulated moisture underneath it, thus changing the SAR response. If that were true it would be very difficult to distinguish changes in soil moisture due to cut grass from other reasons for changes in soil moisture.

Increased soil moisture would increase the relative permittivity of the soil, thus increasing surface scattering and reducing volume scattering from the topmost soil layer. By definition of the scattering alpha angle parameter [102], increased surface backscattering would decrease the alpha angle closer to 0°. In S. Allain's PhD thesis [60], the dominant scattering alpha angle was modelled for X-band SAR according to the IEM soil backscattering model [107]. Similar results were achieved: increased soil moisture decreased the dominant scattering alpha angle [60]. Therefore, accumulated soil moisture under the cut and un-collected grass cannot explain the specific observed behaviour of the scattering alpha angle parameter since a decrease, rather than an increase, should be observed.

3.6. Grassland vegetation modelling

Polarimetric SAR is sensitive to the structural properties of a sensed object. One possible way to explain the observed changes in the scattering alpha angle are through changes in grass plant orientation. When grass was cut its orientation changed from predominantly vertical to predominantly horizontal. In order to test the hypothesis, a random volume over ground model [14] was calculated. The results for different particle shapes are presented in Figure 3.4.

As could be seen from Figure 3.4, horizontal dipoles (grass plants) correspond to higher scattering alpha angles than vertical dipoles. Thus, the changes in grass plant orientation from predominantly vertical to predominantly horizontal could well explain the observed scattering alpha angle increase when grass was cut and left uncollected on the ground.

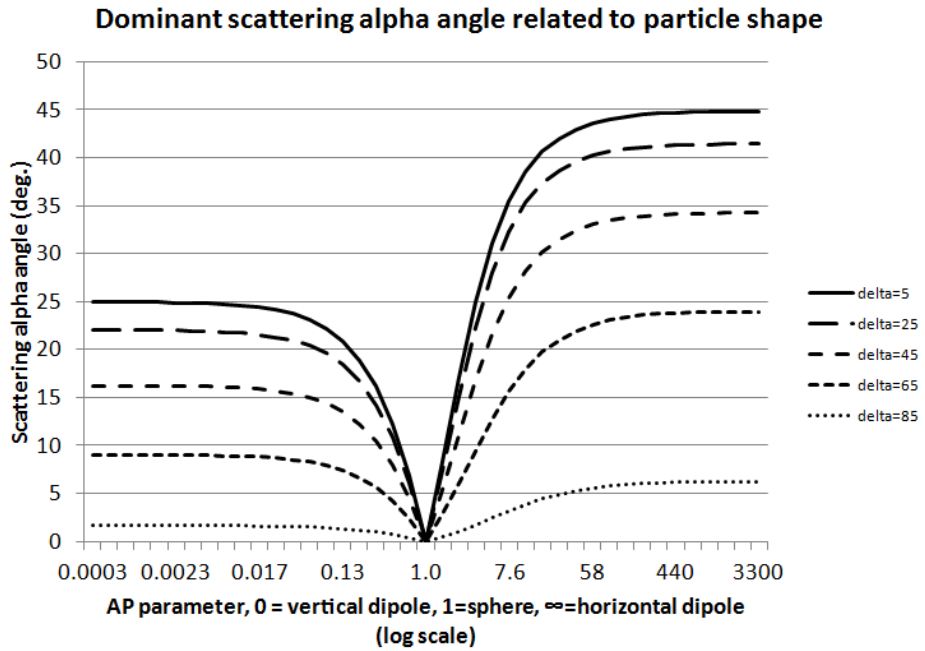

Figure 3.4. Dominant scattering alpha angle according to the random volume over ground vegetation backscattering model [14] for different particle shapes. The delta parameter determines the particles' randomness of orientation: delta=0 corresponds to ideally aligned particles, whereas delta=90 corresponds to completely randomly oriented particles.

4. CONCLUSION

This thesis explores the application of X-band SAR satellite data for environmental monitoring. TerraSAR-X in its single polarisation HH and dual polarisation HH/VV was used as the primary data source. TerraSAR-X data capabilities for forest flood mapping and grassland parameter retrieval applications were studied.

Short 3 cm wavelength X-band SAR HH polarisation data usability for flood mapping in temperate forest areas was tested. Sufficient canopy penetration was observed as flooding increased backscatter in deciduous, mixed and coniferous forest by 6.2, 3.2 and 4.0 dB respectively. The first satellite remote sensing data-based flood maps in Estonia on the Alam-Pedja Nature Reserve were created. These accurate flood maps are a useful source of information for later ecological studies on the Nature Reserve. As the flooded vs. non-flooded forest backscatter difference was sufficient – at least 3.2 dB – X-band SAR systems like TerraSAR-X and COSMO SkyMED could be used for flood mapping in temperate forests. The study confirmed X-band SAR performance for leaf-off conditions, but leaf-on conditions still remain to be tested. However, spring floods from snowmelt occurring during leaf-off conditions are the most common type of flood in Northern Europe. Therefore, X-band SAR usability for flood mapping in Northern Europe during leaf-off conditions could be considered even more important than its usability during leaf-on conditions.

According to SAR polarimetry theory, the HH-VV polarimetric channel should have higher flooded vs. non-flooded area separation based on backscatter values than the HH polarimetric channel. The improvement of using the HH-VV channel was measured at the Soomaa temperate forest test site using TerraSAR-X dual polarimetric HH/VV data with a 23° angle of incidence. The test was done in coniferous and deciduous forests with cover of 75–81% and three different tree height groups: 0–10 m, 10–20 m and 20–30 m. Depending on forest type, the use of the HH-VV channel improved flooded vs. non-flooded forest backscatter-based separation by 0.2–1.6 dB over the conventional HH polarimetric channel. The improvement was at its lowest (0.2 dB) in 7 m tall coniferous forest and at its highest (1.6 dB) in 5–7 m tall deciduous forest. For the HH (HH-VV) polarimetric channel in deciduous forest, flooding increased backscatter by 8.2 (9.8), 7.2 (8.4) and 5.7 dB (6.7 dB) for tree heights 5–7, 14–19 and 20–28 m respectively. In coniferous forest, flooding increased backscatter in the HH (HH-VV) polarimetric channel by 4.8 (5.0), 3.6 (5.0) and 2.3 dB (3.0 dB) for tree heights 7, 16–18 and 23–28 m respectively.

Polarimetric phase difference between the HH and VV channels is another parameter that could be used for flood detection [89]. Flooding increases double-bounce scattering from the surface and tree trunks, and shifts the phase towards 180°. Phase shift was measured using the TerraSAR-X HH/VV Soomaa dataset. In deciduous forest, floods shifted the phase from 59° to 87°, 60° to 83° and 62° to 74° for tree heights 5–7, 14–19 and 20–28 m respectively. In coniferous forest, floods shifted the phase from 59° to 69°, 59° to 70° and

61° to 71° for tree heights 7, 16–18 and 23–28 m respectively. Dual polarimetric HH/VV measurements could be used for improved forest flood mapping, bearing in mind the reduced resolution and/or swath width of dual polarimetric modes compared to single channel modes.

Dual polarimetric HH/VV X-band SAR sensitivity for grassland parameter retrieval was tested. The test was carried out from June to October 2011 in the Matsalu grasslands close to the Baltic Sea coast where grass height varied 5–70 cm in the different test fields. SAR measurements were made with TerraSAR-X in its dual polarimetric HH/VV mode with a mean incidence angle of 36.9°. The SAR observables studied included dual polarimetric entropy, mean and dominant scattering alpha angle, coherence magnitude and phase between HH+VV and HH-VV polarimetric channels, phase magnitude and phase between HH and VV polarimetric channels, |HH|/|VV| intensity ratio, backscatter in HH, VV, HH+VV and HH-VV polarimetric channels. None of the observables were found to be sensitive to grass height, however, one specific behaviour was noticed for the state of cut grass lying on the ground. When the grass was cut and left uncollected horizontally on the ground, the dominant scattering alpha angle increased from 10° to 25°. Characteristic behaviour was also found in the |HH|/|VV| intensity ratio, mean scattering alpha angle, coherence magnitude between HH+VV and HH-VV polarimetric channels and the phase difference between HH and VV polarimetric channels. Such characteristic behaviour for the cut grass lying on the ground was explained using the random volume over ground model for vegetation backscattering [14]. It was shown that primarily horizontally aligned dipoles (grass cut but left uncollected on the ground) corresponded to higher alpha angle values than primarily vertically aligned dipoles (growing grass). The results of the study have applications in precision farming based on satellite measurements and subsidy claim validation in European Union agencies that allocate agricultural subsidies.

In order to search for a SAR parameter sensitive to grass height or biomass and to study further the reasons for the risen alpha angle for cut grass lying on the ground, a new campaign was organised in the summer of 2013. The study included satellite measurements with RADARSAT-2 in its fully polarimetric HH/HV/VH/VV mode, TanDEM-X dual polarimetric HH/VV mode and COSMO SkyMED constellation HH 1-day revisit interferometry mode. The field surveys were also improved, including *in situ* wet and dry biomass, grass height and soil moisture measurements. The results are expected to be published in 2014.

SUMMARY

The research described in this thesis was carried out in Tartu University, Regio Ltd, German Aerospace Center (DLR) and Tartu Observatory between 2010 and 2013. The research focused on testing the capabilities of new generation high-resolution X-band SAR satellites like TerraSAR-X for environmental monitoring.

X-band SAR canopy penetration was found to be sufficient for effective flood mapping in North European temperate forest during leaf-off season. Due to flooding, backscatter increased 6.2, 3.2 and 4.0 dB in deciduous, mixed and coniferous forest respectively. The first high-resolution remote sensing data-based flood maps on the Alam-Pedja Nature Reserve were created. The flood maps could be used as basis for future ecological studies on the Nature Reserve.

The degree of improvement in using the X-band SAR HH-VV polarimetric channel instead of conventional HH for flood mapping in forest areas was measured. In deciduous forest, flooding increased backscatter in the HH (HH-VV) polarimetric channel by 8.2 (9.8), 7.2 (8.4) and 5.7 dB (6.7 dB) for tree heights 5–7, 14–19 and 20–28 m respectively. In coniferous forest, flooding increased backscatter in the HH (HH-VV) polarimetric channel by 4.8 (5.0), 3.6 (5.0) and 2.3 dB (3.0 dB) for tree heights 7, 16–18 and 23–28 m respectively. The improvement in using the HH-VV polarimetric channel over HH was 0.2–1.6 dB, the highest (1.6 dB) being for short 5–7 m deciduous forest and the lowest (0.2 dB) for short 7 m coniferous forest. The corresponding polarimetric phase difference increase between HH and VV channels related to the flooding was measured. In deciduous forest, the phase difference increased from 59° to 87°, 60° to 83° and 62° to 74° for tree heights 5–7, 14–19 and 20–28 m respectively. In coniferous forest, the phase difference increased from 59° to 69°, 59° to 70° and 61° to 71° for tree heights 7, 16–18 and 23–28 m respectively. These results demonstrate the slight improvement of using the HH-VV polarimetric channel for flood mapping in forests instead of the conventional HH channel. However, one also needs to keep in mind that the resolution and/or swath width of dual pol. modes are usually inferior to those of the single channel modes of the same SAR system.

Dual polarimetric HH/VV X-band SAR performance for grasslands parameters retrieval was tested. No reliable correlation between SAR measurements and grass height was observed. However, numerous SAR variables – most notably the dual polarimetric dominant scattering alpha angle – were sensitive to cut grass lying on the ground. A characteristic dominant scattering alpha angle increase from 10° to 25° was observed when grass was cut and left lying on the ground. The alpha angle returned to 10° after the grass was collected. The observed phenomenon was well described by a particle cloud model for vegetation backscattering [14]. Primarily horizontally oriented dipoles (cut grass lying on the ground) correspond to higher scattering alpha angles than primarily vertically oriented dipoles (growing grass).

SUMMARY IN ESTONIAN

X-laineala tehisava-radari rakendused keskkonnakaugseireks

Käesolevas väitekirjas kirjeldatud uurimistöö on läbi viidud Tartu Ülikoolis, AS Regios, Saksa Kosmosekeskuses (DLR) ja Tartu Observatooriumis 2010–2013. Uurimistöö peamiseks eesmärgiks oli kõrglahutusega X-laineala tehisava-radarite rakendusvõimaluste uurimine keskkonnakaugseireks. Lähteandmetena kasutati peamiselt Saksa Kosmosekeskuse satelliidi TerraSAR-X mõõtmisi.

X-laineala tehisava-radari võrastiku läbivus osutus piisavaks, et tuvastada vett ja kaardistada üleujutusi Põhja-Euroopa parasvöötmelises metsas raagus aastaajal. Üleujutus võimendas tagasihajumist leht-, sega- ja okasmetsas vastavalt 6.2, 3.2 ja 4.0 dB. Sama uurimuse raames valmisid ka esimesed kõrglahutusega satelliitkaugseire andmete põhised üleujutuste kaardid Alam-Pedja Looduskaitseala kohta. Loodud üleujutusalade kaarte saab kasutada edasistes geograafia- ja ökoloogia-alastes uurimustes Alam-Pedja Looduskaitseala kohta.

Komplekssе HH-VV polarimeetrilise kanali kasutamine peaks tagasihajumise põhjal pakkuma paremat üleujutatud metsa eristamist üleujutamata metsast, võrreldes traditsioonilise HH kanaliga. TerraSAR-X HH/VV režiimi andmetega Soomaa metsas tehtud mõõtmised näitasid, et tagasihajumise põhine üleujutatud metsa eristatavus üleujutamata metsast suurenes olenevalt metsa tüübist 0.2–1.6 dB HH-VV kanali kasuks võrreldes HH-ga. Kõige rohkem (1.6 dB) paranes eristatavus 5–7 m kõrguses lehtmetsas, kõige vähem (0.2 dB) 7 m okasmetsas. Lehtmetsas suurendas üleujutus HH (HH-VV) kanali tagasihajumist vastavalt 8.2 (9.8), 7.2 (8.4) ja 5.7 dB (6.7 dB) puudel kõrgustega 5–7, 14–19 and 20–28 m. Okasmetsas suurendas üleujutus HH (HH-VV) kanali tagasihajumist vastavalt 4.8 (5.0), 3.6 (5.0) ja 2.3 dB (3.0 dB) puudel kõrgusega 7, 16–18 and 23–28 m. Sama eksperimendi raames mõõdeti ka HH ja VV kanali polarimeetrilist faasivahet, mis on samuti üleujutusele tundlik ning mida on võimalik kasutada üleujutuste kaardistamisel alusparameetrina. Lehtmetsas üleujutamata tingimustel üleujutatud tingimustele üle minnes suurenes HH ja VV kanali faasivahe 28°, 23° ja 12° vastavalt puude kõrgusele 5–7, 14–19 ja 20–28 m. Okasmetsas suurenes samal ajal faasivahe 10°, 11° ja 10° vastavalt puude kõrgusele 7, 16–18 ja 23–28 m. Tulemused näitavad, et HH-VV kanali kasutamine pakub veidi kõrgemat üleujutatud metsa eristamise võimalust üleujutatud metsast, võrreldes traditsioonilise HH kanaliga. Samal ajal tuleb siiski meeles pidada, et kahe polarisatsiooniga tehisava-radarite mõõterežiimide lahutus on veidi jämedam ja/või vaateala kitsam võrreldes sama sensori ühe polarisatsiooniga mõõterežiimiga.

Lisaks testiti kahe kanaliga HH/VV polarimeetrilise tehisava-radari sobivust rohumaade parameetrite tuvastuseks. Ühegi tehisava-radari mõõtetulemuse ja rohu kõrguse vahelist seost ei leitud. Selle asemel osutus võimalikuks kaardistada alasid, kus rohi oli niidetud ja heinamaale maha jäetud. Sellele seisule viitas paljude tehisava-radari mõõtetulemuste iseloomulik käitumine. Kõige

selgem muutus toimus radari hajumise dominantsel alfa-nurgal, mis tõusis rohu niitmise järel 10 kraadilt 25 kraadile, langedes rohu koristamise järel uuesti 10 kraadile. Leitud käitumine vastas hästi osakeste pilve-põhisele taimestiku tagasihajumise mudelile [14]. Peamiselt horisontaalselt paiknevad dipoolid (niidetud ja koristamata rohi põllul) vastasid suuremale alfa-nurgale kui peamiselt vertikaalselt orienteeritud dipoolid (kasvav rohi).

REFERENCES

[1] J. J. McCarthy, Climate change 2001: impacts, adaptation, and vulnerability: contribution of Working Group II to the third assessment report of the Intergovernmental Panel on Climate Change, Cambridge: Cambridge University Press, 2001.

[2] S. Solomon, Climate change 2007-the physical science basis: Working group I contribution to the fourth assessment report of the IPCC, Cambridge: Cambridge University Press, 2007.

[3] Z. W. Kundzewicz, "Flood risk and vulnerability in the changing climate," *Annals of Warsaw University of Life Sciences,* vol. 39, no. 1, pp. 21–30, 2008.

[4] Z. W. Kundzewicz, D. Graczyk, T. Maurer, I. Pińskwar, M. Radziejewski, C. Svensson and M. Szwed, "Trend detection in river flow series: 1. Annual maximum flow," *Hydrological Sciences Journal,* vol. 50, no. 5, pp. 797–810, 2005.

[5] E. W. Cliver, V. Boriakoff and J. Feynman, "Solar variability and climate change: Geomagnetic aa index and global surface temperature.," *Geophysical Research Letters,* vol. 25, no. 7, pp. 1035–1038, 1998.

[6] R. A. Pielke, G. Marland, R. A. Betts, T. N. Chase, J. L. Eastman, J. O. Niles and S. W. Running, "The influence of land-use change and landscape dynamics on the climate system: relevance to climate-change policy beyond the radiative effect of greenhouse gases.," *Philosophical Transactions of the Royal Society of London. Series A: Mathematical, Physical and Engineering Sciences,* vol. 360, no. 1797, pp. 1705–1719, 2002.

[7] J. Schmetz, P. Pili, S. Tjemkes, D. Just, J. Kerkmann, S. Rota and A. Ratier, "An introduction to Meteosat second generation (MSG).," *Bulletin of the American Meteorological Society,* vol. 83, no. 7, pp. 977–992, 2002.

[8] W. L. Barnes, T. S. Pagano and V. V. Salomonson, "Prelaunch characteristics of the moderate resolution imaging spectroradiometer (MODIS) on EOS-AM1.," *IEEE Transactions on Geoscience and Remote Sensing,* vol. 36, no. 4, pp. 1088–1100, 1998.

[9] Commitee of Earth Observation Satellites, "CEOS EO HANDBOOK – CATALOGUE OF SATELLITE MISSIONS," [Online]. Available: http://database.eohandbook.com/. [Accessed 14 December 2013].

[10] Union of Concerned Scientists, "UCS Satellite Database," [Online]. Available: http://www.ucsusa.org/nuclear_weapons_and_global_security/space_weapons/technical_issues/ucs-satellite-database.html. [Accessed 14 December 2013].

[11] NASA, "NASA Spaceflight History," [Online]. Available: http://history.nasa.gov/SP-4202/chap12.html. [Accessed 14 December 2013].

[12] NASA, "The Landsat Program," [Online]. Available: http://landsat.gsfc.nasa.gov/. [Accessed 14 December 2013].

[13] J. Lee and E. Pottier, Polarimetric Radar Imaging – from Basics to Applications, 1st ed., New York: CRC Press, 2009.

[14] S. Cloude, Polarisation: Applications in Remote Sensing, Oxford (USA): Oxford University Press, 2009.

[15] F. M. Henderson and A. J. Lewis, Manual of Remote Sensing: Imaging Radar, New York: John Wiley and Sons, 1998.

[16] C. A. Willey, “Synthetic aperture radars–a paradigm for technology evolution.,” *IEEE Transactions on Aerospace Electronic Systems,* vol. 21, pp. 440–443, 1985.

[17] C. W. Sherwin, J. P. Ruina and R. D. Rawcliffe, “Some Early Developments in Synthetic Aperture Radar Systems,” *IRE Transactions on Military Electronics,* vol. 1051, no. 2, pp. 111–115, 1962.

[18] NASA, “Past Missions – Seasat,” [Online]. Available: http://www3.jpl.nasa.gov/missions/past/seasat.html. [Accessed 26 November 2013].

[19] W. M. Boerner and C. Y. Chan, “Inverse methods in electromagnetic imaging.,” *Medical Application oj Microwave Imaging,* pp. 213–228, 1985.

[20] J. Van Zyl, R. Carande, Y. Lou, T. Miller and K. Wheeler, “The NASA/JPL three-frequency polarimetric AIRSAR system.,” in *Geoscience and Remote Sensing Symposium*, 1992.

[21] S. Martinis, *Automatic near real-time flood detection in high resolution X-band synthetic aperture radar satellite data using context-based classification on irregular graphs. Dissertation der Fakultät für Geowissenschaften der Ludwig-Maximilians-Universität München.,* 2010, pp. 4,22.

[22] M. D. Krohn, N. M. Milton and D. B. Segal, “SEASAT synthetic aperture radar (SAR) response to lowland vegetation types in eastern Maryland and Virginia,” *Journal of Geophysical Research: Oceans ,* vol. 88, no. C3, p. 1937–1952, 1983.

[23] J. L. Place, “Mapping of forested wetlands: Use of Seasat radar images to complement conventional sources,” *Professional Geographer,* vol. 37, no. 4, p. 463−469, 1984.

[24] J. P. Ormsby, B. J. Blanchard and A. J. Blanchard, “Detection of lowland flooding using active microwave systems,” *Photogrammetric Engineering and Remote Sensing,* vol. 51, p. 317–328, 1985.

[25] M. Imhoff, M. Story, C. Vermillion, F. Khan and F. Polcyn, “Forest canopy characterization and vegetation penetration assessment with space-borne radar.,” *IEEE Transactions on Geoscience and Remote Sensing,* vol. 24, no. 4, p. 535–542, 1986.

[26] J. Richards, P. Woodgate and A. Skidmore, “An explanation of enhanced radar backscattering from flooded forests,” *International Journal of Remote Sensing,* vol. 8, no. 7, pp. 1093–1100, 1987.

[27] L. L. Hess, J. M. Melack and D. S. Simonett, “Radar detection of flooding beneath the forest canopy: A review,” *International Journal of Remote Sensing,* vol. 11, no. 7, p. 1313−1325, 1990.

[28] Y. Wang, L. L. Hess, S. Filoso and J. M. Melack, “Understanding the radar backscattering from flooded and non-flooded Amazonian forests: Results from canopy backscatter modeling,” *Remote Sensing of Environment,* vol. 54, no. 3, p. 324−332, 1995.

[29] E. S. Kasischke, J. M. Melaneck and M. C. Dobson, “The use of imaging radars for ecological applications – A review,” *Remote Sensing of Environment,* vol. 59, no. 2, pp. 141–156, 1997.

[30] Y. Wang and M. L. Imhoff, “Simulated and observed L-HH radar backscatter from tropical mangrove forests,” *International Journal of Remote Sensing,* vol. 14, no. 15, p. 2819–2828, 1993.

[31] J. Toyra, A. Pietroniro and L. W. Martz, “Multisensor Hydrologic Assessment of a Freshwater Wetland,” *Remote Sensing of Environment,* vol. 75, no. 2, pp. 162–173, 2001.

[32] L. L. Bourgeau-Chavez, E. S. Kasischke, S. M. Brunzell, J. P. Mudd, K. B. Smith and A. L. Frick, “Analysis of space-borne SAR data for wetland mapping in Virginia riparian ecosystems,” *International Journal of Remote Sensing,* vol. 22, no. 18, pp. 3665–3687, 2001.

[33] J. Henry, P. Chastanet, K. Fellah and Y. Desnos, “ENVISAT multipolarised ASAR data for flood mapping,” in *Proceedings of the IEEE International Geoscience and Remote Sensing Symposium*, Toulouse, France, 2003.

[34] Y. Dong and J. A. Richards, “Studies of the cylinder-ground double bounce scattering mechanism in forest backscatter models,” *IEEE Transactions on Geoscience and Remote Sensing,* vol. 33, no. 1, pp. 229 - 231, 1995.

[35] P. A. Townsend, “Mapping seasonal flooding in forested wetlands using multi-temporal radarsat SAR,” *Photogrammetric Engineering and Remote Sensing,* vol. 67, no. 7, p. 857−864, 2001.

[36] M. W. Lang, P. A. Towsend and E. S. Kasischke, “Influence of incidence angle on detecting flooded forests using C-HH synthetic aperture radar data,” *Remote Sensing of Environment,* vol. 112, p. 3898–3907, 2008.

[37] F. M. Henderson, “Environmental factors and the detection of open surface water areas with X-band radar imagery,” *International Journal of Remote Sensing,* vol. 16, no. 13, pp. 2423–2437, 1995.

[38] K. Voormansik, J. Praks, O. Antropov, J. Jagomägi and K. Zalite, “Flood Mapping With TerraSAR-X in Forested Regions in Estonia,” *IEEE Journal of Selected Topics in Applied Earth Observations and Remote Sensing ,* vol. in print, 2013.

[39] L. Marinelli, R. Michel, A. Beaudoin and J. Astier, “Flood mapping using ERS tandem coherence image: a case study in south France,” in *Proceedings of the 3rd ERS Symposium*, Florence, Italy, 1997.

[40] C. Buck and S. Monni, “Application of SAR Interferometry to Flood Damage Assessment,” in *SAR Workshop, Committee on Earth Observation Satellites*, Toulouse, France, 1999.

[41] G. Nico, M. Pappalepore, G. Pasquariello, S. Refice and S. Samarelli, “Comparison of SAR amplitude vs. coherence flood detection methods – a GIS application,” *International Journal of Remote Sensing,* vol. 21, no. 8, p. 1619–1631, 2000.

[42] S. Dellepiane, G. Bo, S. Monni and C. Buck, “SAR images and interferometric coherence for flood monitoring,” in *Proceedings of the IEEE Geoscience and Remote Sensing Symposium*, Honolulu, HI , USA, 2000.

[43] V. Herrera-Cruz and F. Koudogbo, “TerraSAR-X Rapid Mapping for Flood Events,” in *Intenrnational Society for Photogrammetry and Remote Sensing Workshop*, Hannover, Germany, 2009.

[44] M. Silveira and S. Heleno, “Separation between water and land in SAR images using region-based level sets,” *IEEE Geoscience and Remote Sensing Letters,* vol. 6, no. 3, p. 471–475, 2009.

[45] S. Martinis, A. Twele and V. S., “Towards operational near real-time flood detection using a split-based automatic thresholding procedure on high resolution TerraSAR-X data,” *Natural Hazards and Earth System Sciences,* vol. 9, pp. 303–314, 2009.

[46] S. Martinis, A. Twele and S. Voigt, “Unsupervised extraction of flood-induced backscatter changes in SAR data using Markov image modeling on irregular graphs,” *IEEE Transactions on Geoscience and Remote Sensing,* vol. 49, no. 1, pp. 251–263, 2011.

[47] D. C. Mason, R. Speck, B. Devereux, G. J.-P. Schumann, J. C. Neal and B. P. D., “Flood Detection in Urban Areas Using TerraSAR-X,” *IEEE Transactions on Geoscience and Remote Sensing,* vol. 48, no. 2, pp. 882–894, 2010.

[48] D. C. Mason, I. J. Davenport, J. C. Neal, G. J.-P. Schumann and P. D. Bates, “Near real-time flood detection in urban and rural areas using high-resolution synthetic aperture radar images,” *IEEE Transactions on Geoscience and Remote Sensing,* vol. 50, no. 8, pp. 3041 - 3052, 2012.

[49] C. Anderson, *Ecology and Management of the Praire Division,* 2008.

[50] Y. C. Lu, C. Daughtry, G. Hart and B. Watkins, “The current state of precision farming.,” *Food reviews international,* vol. 13, no. 2, pp. 141–162, 1997.

[51] R. Sylvester-Bradley, E. Lord, D. L. Sparkes, R. K. Scott, J. J. J. Wiltshire and J. Orson, “An analysis of the potential of precision farming in Northern Europe.,” *Soil use and management ,* vol. 15, no. 1, pp. 1–8, 1999.

[52] A. Luckman, “The Effects of Topography on Mechanisms of Radar Backscatter from Coniferous Forest and Upland Pasture,” *IEEE Transactions on Geoscience and Remote Sensing,* vol. 36, no. 5, pp. 1830–1834, 1998.

[53] M. J. Hill, G. E. Donald and P. J. Vickery, “Relating Radar Backscatter to Biophysical Properties of Temperate Perennial Grassland,” *Remote Sensing of Environment,* vol. 67, no. 1, pp. 15–31, 1999.

[54] M. Herold, C. C. Schmullius and I. Hajnsek, “Multifrequency and Polarimetric Radar Remote Sensing of Grassland - Geobiophysical and Landcover Parameter Retrieval with E-SAR Data,” 2001.

[55] N. Mino, G. Saito and S. Ogawa, “Detecting management practices of improved grasslands using ERS-1 SAR data,” in *ACRS*, 1997.

[56] B. Bouman and H. van Kasteren, “Ground-Based X-Band (3-cm Wave) Radar Backscattering of Agricultural Crops. II. Wheat, Barley, and Oats; the Impact of Canopy Structure,” *Remote Sensing of Environment,* vol. 34, pp. 107–119, 1990.

[57] B. Bouman and D. Hoekman, “Multi-temporal, multi-frequency radar measurements of agricultural crops during the Agriscatt-88 campaign in The Netherlands,” *International Journal of Remote Sensing,* vol. 14, no. 8, pp. 1595–1614, 1993.

[58] F. Ulaby and P. Batlivala, “Optimum radar parameters for mapping soil moisture,” *IEEE Transactions on Geoscience and Remote Sensing,* vol. 14, pp. 81–93, 1976.

[59] I. Hajnsek, E. Pottier and S. R. Cloude, “Inversion of Surface Parameters From Polarimetric SAR,” *IEEE Transactions on Geoscience and Remote Sensing,* vol. 41, no. 4, pp. 727–744, 2003.

[60] S. Allain, “CARACTERISATION POLARIMETRIQUE D’UN SOL - MULTI-FREQUENCES,” in *Caractérisation d’un sol nu à partir de données SAR polarimétriques*, Rennes, 2003, p. 118.

[61] A. Fung and F. Ulaby, “Matter-energy interactions in the microwave region,” in *Manual of remote sensing 2nd ed.*, R. Colwell, Ed., Falls Church, American Society of Photogrammetry, 1983, p. 1232.

[62] K. Sarabandi, Y. Oh and F. Ulaby, “Polarimetric radar measurements of bare soil surfaces at microwave frequencies,” 1991.

[63] B. Brisco, R. Brown, B. Snider, G. Sofko, J. Köhler and A. Wacker, “Tillage effects on the radar backscattering coefficient of grain stubble fields,” *International Journal of Remote Sensing,* vol. 12, pp. 2283–2298, 1991.

[64] H. McNairn, J. Boisvert, D. Major, Q. Gwyn, R. Brown and S. A.M., “Identification of agricultural tillage practices from C-band radar backscatter,” *Canadian Journal of Remote Sensing,* vol. 22, pp. 154–162, 1996.

[65] A. Beaudoin, T. Le Toan and Q. Gwyn, “SAR observations and modeling of the C-band backscatter variability due to multiscale geometry and soil moisture,” *IEEE Transactions on Geoscience and Remote Sensing,* vol. 28, pp. 886–895, 1990.

[66] R. Raney, “Radar fundamental: technical perspectiver,” in *Principles and applications of imaging radar, manual of remote sensing 3rd ed.*, F. Henderson and A. Lewis, Eds., New York, John Wiley & Sons, 1998, pp. 9–130.

[67] P. Ferrazzoli, L. Guerriero and G. Schiavon, “Experimental and model investigation on radar classification capability,” *IEEE Transactions on Geoscience and Remote Sensing,* vol. 37, pp. 960–968, 1999.

[68] H. McNairn and B. Brisco, “The application of C-band polarimetric SAR for agriculture: a review,” *Canadian Journal of Remote Sensing,* vol. 30, no. 3, pp. 525–542, 2004.

[69] G. Bradley and F. Ulaby, “Aircraft radar response to soil moisture,” *Remote Sensing of Environment,* vol. 11, pp. 419–438, 1981.

[70] H. McNairn, C. Duguay, J. Boisvert, E. Huffman and B. Brisco, “Defining the sensitivity of multi-frequency and multi-polarized radar backscatter to post-harvested crop residue,” *Canadian Journal of Remote Sensing,* vol. 27, pp. 247–263, 2001.

[71] S. Buckreuss, W. Balzer, P. Muhlbauer, R. Werninghaus and W. Pitz, “The TerraSAR-X satellite project.,” in *Proceedings of Geoscience and Remote Sensing Symposium*, 2003.

[72] F. Covello, F. Battazza, A. Coletta, E. Lopinto, C. Fiorentino, L. Pietranera and S. Zoffoli, “COSMO-SkyMed an existing opportunity for observing the Earth.,” *Journal of Geodynamics,* vol. 49, no. 3, pp. 171–180, 2010.

[73] T. Fritz and M. Eineder, “TerraSAR-X Basic Product Specification Document,” 15 10 2010. [Online]. Available: http://sss.terrasar-x.dlr.de/pdfs/TX-GS-DD-3302.pdf. [Accessed 16 03 2012].

[74] Agenzia Spaziale Italiana/Italian Space Agency, "COSMO SkyMed SAR PRODUCTS HANDBOOK," [Online]. Available: http://www.cosmo-skymed.it/docs/ASI-CSM-ENG-RS-092-A-CSKSARProductsHandbook.pdf. [Accessed 26 November 2013].

[75] W.-M. Boerner and M. El-Arini, "Polarization dependence in electromagnetic inverse problem," *IEEE Transactions on Antennas and Propagation,* vol. 29, no. 2, p. 262–271, 1981.

[76] W.-M. Boerner, "Use of Polarization in Electromagnetic Inverse Scattering," *Radio Science,* vol. 16, no. 6, p. 1037–1045, 1981.

[77] J. D. Jackson, Classical Electrodynamics, New York: Wiley and Sons, 1999.

[78] T. Meissner and F. J. Wentz, "The complex dielectric constant of pure and sea water from microwave satellite observations.," *IEEE Transactions on Geoscience and Remote Sensing,* vol. 42, no. 9, pp. 1836–1849, 2004.

[79] M. Norimoto, "Dielectric Properties of Wood," *Wood research: bulletin of the Wood Research Institute Kyoto University,* vol. 59, pp. 106–152, 1976.

[80] C. Mätzler and A. Murk, "Complex dielectric constant of dry sand in the 0.1 to 2 GHz range," University of Bern, Bern, 2010.

[81] S. Fujita, T. Matsuoka, T. Ishida, K. Matsuoka and S. Mae, "A summary of the complex dielectric permittivity of ice in the megahertz range and its applications for radar sounding of polar ice sheets," *Physics of Ice Core Records,* pp. 185–212, 2000.

[82] P. A. Townsend, "Relationships between forest structure and the detection of flood inundation in forested wetlands using C-band SAR," *International Journal of Remote Sensing,* vol. 23, no. 3, p. 443−460, 2002.

[83] I. G. Cumming and F. H. Wong, Digital signal processing of synthetic aperture radar data: algorithms and implementation., Norwood: Artech House, 2004.

[84] EMHI (Estonian Meteorological and Hydrological Institute), "Real time water level in Estonian rivers," 2010. [Online]. Available: http://www.emhi.ee/index.php?ide=21,466. [Accessed 6 August 2010].

[85] EME (Estonian Ministry of the Environment), "Estonian Forestry Register (Eesti Metsaregister)," 2011. [Online]. Available: http://register.metsad.ee/avalik. [Accessed 27 January 2011].

[86] R. Treuhaft, F. Goncalves, S. Madsen, J. R. d. Santos, M. Palace, M. Keller, S. Hensley and P. M. L. d. Alencastro Graca, "Tropical Forest Remote Sensing of Structure and Biomass over Brazil with TanDEM-X," in *TanDEM-X Science Team Meeting*, Oberpfaffenhofen, 2013.

[87] S. Cloude, "Group theory and polarization algebra," *Optik,* vol. 75, no. 1, pp. 26–36, 1986.

[88] J. Stratton, Electromagnetic Theory, New York: McGraw-Hill, 1941.

[89] M. S. Horritt, D. C. Mason, D. M. Cobby, I. J. Davenport and P. Bates, "Waterline mapping in flooded vegetation from airborne SAR imagery," *Remote Sensing of Environment,* vol. 85, no. 3, pp. 271–281, 2003.

[90] J. Lee, D. Schuler, R. Lang and K. Ranson, "K-distribution for multi-look processed polarimetric SAR imagery," in *Proceedings of IGARSS'94*, Pasadena, 1994.

[91] JAXA, "ALOS/PALSAR Level 1.1/1.5 product Format description," [Online]. Available: http://www.eorc.jaxa.jp/ALOS/en/doc/fdata/PALSAR_x_ Format_EL.pdf. [Accessed 7 December 2013].

[92] G. F. D. Grandi, P. Mayaux, J. P. Malingreau, A. Rosenqvist, S. Saatchi and M. Simard, "New Perspectives on Global Ecosystems from Wide-Area Radar Mosaics. Flooded Forest Mapping in the Tropics," *International Journal of Remote Sensing,* vol. 21, no. 6–7, pp. 1235–1249, 2000.

[93] M. S. Horritt, D. C. Mason and A. J. Luckman, "Flood boundary delineation from synthetic aperture radar imagery using a statistical active contour model," *International Journal of Remote Sensing,* vol. 22, no. 13, pp. 2489–2507, 2001.

[94] Estonian Land Board, "X-GIS Public Webmap Service," [Online]. Available: http://xgis.maaamet.ee/xGIS/XGis. [Accessed 16 03 2012].

[95] J.-S. Lee, "Refined filtering of image noise using local statistics.," *Computer graphics and image processing,* vol. 15, no. 4, pp. 380–389, 1981.

[96] M. Hill, C. Ticehurst, J. Lee, M. Grunes, G. Donald and D. Henry, "Integration of Optical and Radar Classification for Mapping Pasture Type in Western Australia," *IEEE Transactions on Geoscience and Remote Sensing,* vol. 43, no. 7, pp. 1665–1681, 2005.

[97] M. A. Friedl, D. S. Schimel, J. Michaelsen, F. W. Davis and H. Walker, "Estimating grassland biomass and leaf area index using ground and satellite data.," *International Journal of Remote Sensing,* vol. 15, no. 7, pp. 1401–1420, 1994.

[98] Y. Xie, Z. Sha, M. Yu, Y. Bai and L. Zhang, "A comparison of two models with Landsat data for estimating above ground grassland biomass in Inner Mongolia," *Ecological Modelling,* vol. 220, no. 15, pp. 1810–1818, 2009.

[99] A. Freeman and S. Durden, "A three-component scattering model for polarimetric SAR data," *IEEE Transactions on Geoscience and Remote Sensing,* vol. 36, no. 3, pp. 963–973, 1998.

[100] M. Schwerdt, D. Schrank, M. Bachmann, C. Schulz, B. Doering and J. Hueso Gonzales, "TerraSAR-X Re-Calibration and Dual Receive Antenna Campaigns performed in 2009," in *8th European Conference on Synthetic Aperture Radar*, Aachen, 2010.

[101] S. Cloude, "Target decomposition theorems in radar scattering," *Electronics Letters,* vol. 21, no. 1, pp. 22–24, 1985.

[102] S. Cloude and E. Pottier, "An entropy based classification scheme for land applications of polarimetric SAR," *IEEE Transactions on Geoscience and Remote Sensing,* vol. 35, no. 1, pp. 68–78, 1997.

[103] S. R. Cloude, "The dual polarization entropy/alpha decomposition: a PALSAR case study," in *PolInSAR2007 Workshop*, Frascati, 2007.

[104] J. M. Lopez-Sanchez, B.-B. J.D. and I. Hajnsek, "First Results of Rice Monitoring Practices in Spain by Means of Time Series of TerraSAR-X Dual-Pol Images," *IEEE Journal of Selected Topics in Applied Earth Observations and Remote Sensing,* vol. 4, no. 2, pp. 412–422, 2011.

[105] Estonian Meteorological and Hydrological Insitute, "Last 24 hour precipitation sums of Estonian meteorological and hydrological stations.," 3 6 2012. [Online]. Available: http://www.emhi.ee/index.php?ide=21,328,469&liigu=2011-06-07&gtund=8. [Accessed 3 6 2012].

[106] Estonian Meteorological and Hydrological Institute , “Weather observations,” 2011. [Online]. Available: http://www.emhi.ee/index.php?ide=21&v_kiht=2. [Accessed 15 03 2012].

[107] A. K. Fung, Z. Li and K. S. Chen, “Backscattering from a randomly rough dielectric surface,” *IEEE Transactions on Geoscience and Remote Sensing,* vol. 30, no. 2, pp. 356–369, 1992.

ACKNOWLEDGEMENTS

This thesis and the beginning of my researcher journey have only been possible thanks to many good people. First of all I would like to thank my parents and family. Since I was very young I had very interesting talks with my father Peedu about geography, technological development and sense of living. My mother has always provided me support and taught how to keep my things in good order and finish everything I had started. I would also like to thank my grandmother Mamma, who started to teach me numbers and writing when I was 3 years old and was my biggest fan as long as she lived. My sister Kadri and brothers Tanel and Villem have always been my best friends. I am grateful to my girl Siiri for being always very supportive, understanding and ready to listen to my worries throughout my whole doctoral study years.

I would like to thank my supervisors Mart Noorma and Rein Rõõm. Mart has been a very special person, I am very happy for the chance to work with him. His positive attitude, forgivingness, friendliness and courage to set high goals have influenced me a lot. I am also grateful to Mart for his readiness to always support and solve my problems. I also value my second supervisor Rein Rõõm's views a lot to always think critically and work carefully which is equally important to positive attitude and friendliness. The work in the Estonian student satellite team has a special meaning for me, I am happy for the chance to work in a group of very enthusiastic, young and clever people starting with Silver Lätt, Viljo Allik, Urmas Kvell, Riho Vendt, Mihkel Pajusalu and many others. I am thankful to Teet and Jüri Jagomägi for the Regio years. Teet's willingness to attack challenging problems, the art to motivate people, including me, is something I would like to carry on. Discussions with Jüri Jagomägi have been very interesting, he has provided a lot of good ideas, of which I have time to realize only a fraction. I am glad to have such talented, hard-working and deliberative colleagues like Aire and Karlis. I would also like to thank Jaan Praks for being my first instructor into the world of SAR and Peeter Saari for operative answers for my various signal processing and physics related questions during my doctoral study years. Special thanks to Thomas Jagdhuber and Jun Su Kim from German Aerospace Center (DLR). It has been a joy to work with Thomas on the grasslands parameters retrieval as he has always provided me super fast and relevant feedback and suggested ideas how to bring our study further. Thanks to Jun Su I learned many important SAR and signal processing concepts during my tutorial months in DLR, his answers to my questions were always very short, but straight to the point. I would also like to thank the PolInSAR group leaders Kostas Papathanassiou and Irena Hajnsek for the opportunity to work in DLR and take my knowledge about SAR to the next level. Last, but not least I would like to thank Francisco (Paco) Lopez-Dekker from DLR, who I first met during the ESA SAR Remote Sensing Course in Warsaw in September 2010. Paco's teaching about SAR was very inspiring and later he has always had time to give good advice and helped to realise my dream to come and work some months in DLR on SAR.

The following public institutions and companies also played an important role in helping to realise the thesis. I would like to thank Regio Ltd for being a patient and flexible employer as some months I had very little time to work and a lot of time to study. Regio also provided various geospatial data and geo-informatical expertise for the data processing especially during the first years of my doctoral studies. Thanks to Tartu Observatory and its friendly director Anu Reinart for the research facilities and financial support needed to finish my thesis and to develop our SAR workgroup to a powerful scientific team in Europe in near future. I would like to thank DLR for the TerraSAR-X and TanDEM-X data used in the research distributed under project HYD0733, LAN1123, NTI_INSA1194 and NTI_POLI2174. Thanks to ESA and Francesco Sarti for the ENVISAT ASAR and ALOS PALSAR data used in the thesis. Thanks to Estonian Agricultural Registers and Information Board and its enthusiastic remote sensing group leader Kai Raudvere for the geospatial data and advice needed to realise the grasslands experiments of the thesis and also for the open attitude for new experiments and innovations.

Successful doctoral studies are only possible after successful master studies. I am grateful to Skype, Estonian Information Technology Foundation, Foundation Archimedes and European Space Agency for the scholarships that helped to realize my dreams to study in the International Space University (ISU), Strasbourg, France. The ISU year proved later very useful by giving the big picture of space science and space business, taught me management and learning skills.

The doctoral studies were supported by DoRa T3 scholarship “Doktoritöö osaliselt väljaspool ülikooli”. The research visit to DLR was supported by DoRa T6 and Kristjan Jaak scholarships.

PUBLICATIONS

CURRICULUM VITAE

Name: Kaupo Voormansik
Date of birth: February 7, 1985, Viiratsi, Estonia
Citizenship: Estoninan
Address: Tartu Observatory
61602, Tõravere
Tartumaa, Estonia
E-mail: kaupo.voormansik@ut.ee
Phone: +372 5666 9225

Education:

2010–2014 University of Tartu, PhD studies
2008–2009 International Space University, France, MSc (space studies)
2007–2009 University of Tartu, MSc (information technology)

Languages:

Estonian (mother-tongue), English (fluent), German (intermediate), Russian (basic)

Professional employment:

2009–... AS Regio, space technologies specialist
2009–… University of Tartu, lecturer in subjects "Space Technology Basics" and "Fundamentals of Signals and Systems I"
2011–2012 German Aerospace Center (DLR), visiting researcher

Scientific and research activity:

Natural Sciences and Engineering – Radar Remote Sensing

Rewards and scholarships:

08.2011 Foundation Archimedes "DoRa T6" scholarship for Synthetic Aperture Radar studies in German Aerospace Center (DLR) (4 731.– EUR)
08.2011 Foundation Archimedes "Kristjan Jaak" scholarship for Synthetic Aperture Radar studies in German Aerospace Center (DLR) (1 950.– EUR)
08.2008 Skype scholarship for M.Sc studies in International Space University (100 000.– EEK, grantors: Skype and Estonian Information Technology Foundation)
08.2008 Foundation Archimedes "Kristjan Jaak" scholarship for MSc studies in International Space University (164 000.– EEK)
07.2008 European Space Agency scholarship for tution fees in International Space University (18 000.– EUR)

Supervised dissertations:

2013 Villem Voormansik, BSc, (sup) Kaupo Voormansik, (sup) Raivo Aunap, "Maapinna ja majade vertikaalliikumise mõõtmine Tartu linnas PSInSAR meetodil (Measuring buildings and land subsidence in Tartu with PSInSAR technique)", University of Tartu

2013 Iris Laatsarus, BSc, (sup) Kaupo Voormansik, "Metsatüüpide eristamise võimalustest multispektraalsete WorldView-2 satelliidipiltide abil (About the possibilities of forest types classification with WorldView-2 multispectral satellite images)", University of Tartu

2011 Martynas Pelakauskas, MSc, 2010, (sup) Mart Noorma, (sup) Viljo Allik, (sup) Kaupo Voormansik, "ESTCube-1 satellite electrical power system battery subsystem design and testing (ESTCube-1 satelliidi elektrisüsteemi aku alamsüsteemi disain ja testimine)", University of Tartu

2010 Urmas Kvell, MSc, (sup) Mart Noorma, (sup) Kaupo Voormansik, (sup) Viljo Allik, "ESTCube-1 satellite beacon (ESTCube-1 satelliidi raadiomajakas)", University of Tartu

Other Activities:

2004–… Member of fraternity Vironia

2006–… Member of orienteering club LSF PT, participating in and organizing orienteering competitions

Publications:

1. K. Voormansik, T. Jagdhuber, A. Olesk, I. Hajnsek and K. P. Papahtanassiou, "Towards a detection of grassland cutting practices with dual polarimetric TerraSAR-X data," International Journal of Remote Sensing, vol. 34, no. 22, pp. 8081–8103, 2013.
2. K. Voormansik, J. Praks, O. Antropov, J. Jagomägi and K. Zalite, "Flood Mapping With TerraSAR-X in Forested Regions in Estonia," IEEE Journal of Selected Topics in Applied Earth Observations and Remote Sensing , vol. in print, 2013.
3. K. Zalite, K. Voormansik, A. Olesk, M. Noorma and R. A., "Effects of Inundated Vegetation on X-Band HH–VV Backscatter and Phase Difference," IEEE Journal of Selected Topics in Applied Earth Observations and Remote Sensing, vol. in print, 2013.
4. K. Voormansik, T. Jagdhuber, I. Hajnsek and K. P. Papathanassiou, "Improving Semi-natural Grassland Administration with TerraSAR-X," in Proceedings of the 17th GeoCAP Annual Conference, Tallinn, 2011.

ELULOOKIRJELDUS

Nimi: Kaupo Voormansik
Sünniaeg: 7. veebruar, 1985, Viiratsi, Eesti
Kodakondsus: Eesti
Aadress: Tartu Observatoorium
61602, Tõravere
Tartumaa, Eesti
E-post: kaupo.voormansik@ut.ee
Telefon: +372 5666 9225

Haridus:

2010–2014	Tartu Ülikool, doktorant
2008–2009	Rahvusvaheline Kosmoseülikool, Prantsusmaa, MSc (kosmosetehnoloogia)
2007–2009	Tartu Ülikool, MSc (infotehnoloogia)

Keeleoskus:
Eesti (emakeel), inglise (sorav), saksa (kesktase), vene (algtase)

Teenistuskäik:

2009–...	AS Regio, kosmosetehnoloogiate spetsialist
2009–…	Tartu Ülikool, lektor ainetes „Kosmosetehnoloogia alused" and „Signaalitöötluse alused I"
2011–2012	Saksa Kosmosekeskus (DLR), külalisteadlane

Teadus- ja arendustegevus:
Loodusteadused ja tehnika – radarkaugseire

Stipendiumid:

08.2011	Sihtasutus Archimedese „DoRa T6" stipendium tehisava-radari alaseks uurimistööks Saksa Kosmosekeskuses (DLR) (4 731.– EUR)
08.2011	Sihtasutus Archimedese „Kristjan Jaagu" stipendium tehisava-radari alaseks uurimistööks Saksa Kosmosekeskuses (DLR) (1 950.– EUR)
08.2008	Skype stipendium õppemaksu tasumiseks Rahvusvahelises Kosmoseülikoolis (100 000.– EEK, annetajad: Skype ja Eesti Infotehnoloogia Sihtasutus)
08.2008	Sihtasutus Archimedese „Kristjan Jaagu" stipendium õpinguteks Rahvusvahelises Kosmoseülikoolis (164 000.– EEK)
07.2008	Euroopa Kosmoseagentuuri stipendium õppemaksu tasumiseks Rahvusvahelises Kosmoseülikoolis (18 000.– EUR)

Juhendatud väitekirjad:

2013 Villem Voormansik, BSc, juhendajad Kaupo Voormansik ja Raivo Aunap, "Maapinna ja majade vertikaalliikumise mõõtmine Tartu linnas PSInSAR meetodil (Measuring buildings and land subsidence in Tartu with PSInSAR technique)", Tartu Ülikool

2013 Iris Laatsarus, BSc, juhendaja Kaupo Voormansik, "Metsatüüpide eristamise võimalustest multispektraalsete WorldView-2 satelliidipiltide abil (About the possibilities of forest types classification with WorldView-2 multispectral satellite images)", Tartu Ülikool

2011 Martynas Pelakauskas, MSc, 2010, juhendajad Mart Noorma, Viljo Allik ja Kaupo Voormansik, "ESTCube-1 satellite electrical power system battery subsystem design and testing (ESTCube-1 satelliidi elektrisüsteemi aku alamsüsteemi disain ja testimine)", Tartu Ülikool

2010 Urmas Kvell, MSc, juhendajad Mart Noorma, Kaupo Voormansik ja Viljo Allik, "ESTCube-1 satellite beacon (ESTCube-1 satelliidi raadiomajakas)", Tartu Ülikool

Muu tegevus:

2004–… Korporatsioon Vironia liige

2006–… Orienteerumisklubi LSF PT liige

Publikatsioonid:

1. K. Voormansik, T. Jagdhuber, A. Olesk, I. Hajnsek and K. P. Papahtanassiou, "Towards a detection of grassland cutting practices with dual polarimetric TerraSAR-X data," International Journal of Remote Sensing, vol. 34, no. 22, pp. 8081–8103, 2013.
2. K. Voormansik, J. Praks, O. Antropov, J. Jagomägi and K. Zalite, "Flood Mapping With TerraSAR-X in Forested Regions in Estonia," IEEE Journal of Selected Topics in Applied Earth Observations and Remote Sensing , vol. in print, 2013.
3. K. Zalite, K. Voormansik, A. Olesk, M. Noorma and R. A., "Effects of Inundated Vegetation on X-Band HH–VV Backscatter and Phase Difference," IEEE Journal of Selected Topics in Applied Earth Observations and Remote Sensing, vol. in print, 2013.
4. K. Voormansik, T. Jagdhuber, I. Hajnsek and K. P. Papathanassiou, "Improving Semi-natural Grassland Administration with TerraSAR-X," in Proceedings of the 17th GeoCAP Annual Conference, Tallinn, 2011.

DISSERTATIONES PHYSICAE UNIVERSITATIS TARTUENSIS

1. **Andrus Ausmees.** XUV-induced electron emission and electron-phonon interaction in alkali halides. Tartu, 1991.
2. **Heiki Sõnajalg.** Shaping and recalling of light pulses by optical elements based on spectral hole burning. Tartu, 1991.
3. **Sergei Savihhin.** Ultrafast dynamics of F-centers and bound excitons from picosecond spectroscopy data. Tartu, 1991.
4. **Ergo Nõmmiste.** Leelishalogeniidide röntgenelektronemissioon kiiritamisel footonitega energiaga 70–140 eV. Tartu, 1991.
5. **Margus Rätsep.** Spectral gratings and their relaxation in some low-temperature impurity-doped glasses and chrystals. Tartu, 1991.
6. **Tõnu Pullerits.** Primary energy transfer in photosynthesis. Model calculations. Tartu, 1991.
7. **Olev Saks.** Attoampri diapasoonis voolude mõõtmise füüsikalised alused. Tartu, 1991.
8. **Andres Virro.** AlGaAsSb/GaSb heterostructure injection lasers. Tartu, 1991.
9. **Hans Korge.** Investigation of negative point discharge in pure nitrogen at atmospheric pressure. Tartu, 1992.
10. **Jüri Maksimov.** Nonlinear generation of laser VUV radiation for high-resolution spectroscopy. Tartu, 1992.
11. **Mark Aizengendler.** Photostimulated transformation of aggregate defects and spectral hole burning in a neutron-irradiated sapphire. Tartu, 1992.
12. **Hele Siimon.** Atomic layer molecular beam epitaxy of A^2B^6 compounds described on the basis of kinetic equations model. Tartu, 1992.
13. **Tõnu Reinot.** The kinetics of polariton luminescence, energy transfer and relaxation in anthracene. Tartu, 1992.
14. **Toomas Rõõm.** Paramagnetic H^{2-} and F^+ centers in CaO crystals: spectra, relaxation and recombination luminescence. Tallinn, 1993.
15. **Erko Jalviste.** Laser spectroscopy of some jet-cooled organic molecules. Tartu, 1993.
16. **Alvo Aabloo.** Studies of crystalline celluloses using potential energy calculations. Tartu, 1994.
17. **Peeter Paris.** Initiation of corona pulses. Tartu, 1994.
18. **Павел Рубин.** Локальные дефектные состояния в CuO_2 плоскостях высокотемпературных сверхпроводников. Тарту, 1994.
19. **Olavi Ollikainen.** Applications of persistent spectral hole burning in ultrafast optical neural networks, time-resolved spectroscopy and holographic interferometry. Tartu, 1996.
20. **Ülo Mets.** Methodological aspects of fluorescence correlation spectroscopy. Tartu, 1996.
21. **Mikhail Danilkin.** Interaction of intrinsic and impurity defects in CaS:Eu luminophors. Tartu, 1997.

22. **Ирина Кудрявцева.** Создание и стабилизация дефектов в кристаллах KBr, KCl, RbCl при облучении ВУФ-радиацией. Тарту, 1997.
23. **Andres Osvet.** Photochromic properties of radiation-induced defects in diamond. Tartu, 1998.
24. **Jüri Örd.** Classical and quantum aspects of geodesic multiplication. Tartu, 1998.
25. **Priit Sarv.** High resolution solid-state NMR studies of zeolites. Tartu, 1998.
26. **Сергей Долгов.** Электронные возбуждения и дефектообразование в некоторых оксидах металлов. Тарту, 1998.
27. **Kaupo Kukli.** Atomic layer deposition of artificially structured dielectric materials. Tartu, 1999.
28. **Ivo Heinmaa.** Nuclear resonance studies of local structure in $RBa_2Cu_3O_{6+x}$ compounds. Tartu, 1999.
29. **Aleksander Shelkan.** Hole states in CuO_2 planes of high temperature superconducting materials. Tartu, 1999.
30. **Dmitri Nevedrov.** Nonlinear effects in quantum lattices. Tartu, 1999.
31. **Rein Ruus.** Collapse of 3d (4f) orbitals in 2p (3d) excited configurations and its effect on the x-ray and electron spectra. Tartu, 1999.
32. **Valter Zazubovich.** Local relaxation in incommensurate and glassy solids studied by Spectral Hole Burning. Tartu, 1999.
33. **Indrek Reimand.** Picosecond dynamics of optical excitations in GaAs and other excitonic systems. Tartu, 2000.
34. **Vladimir Babin.** Spectroscopy of exciton states in some halide macro- and nanocrystals. Tartu, 2001.
35. **Toomas Plank.** Positive corona at combined DC and AC voltage. Tartu, 2001.
36. **Kristjan Leiger.** Pressure-induced effects in inhomogeneous spectra of doped solids. Tartu, 2002.
37. **Helle Kaasik.** Nonperturbative theory of multiphonon vibrational relaxation and nonradiative transitions. Tartu, 2002.
38. **Tõnu Laas.** Propagation of waves in curved spacetimes. Tartu, 2002.
39. **Rünno Lõhmus.** Application of novel hybrid methods in SPM studies of nanostructural materials. Tartu, 2002.
40. **Kaido Reivelt.** Optical implementation of propagation-invariant pulsed free-space wave fields. Tartu, 2003.
41. **Heiki Kasemägi.** The effect of nanoparticle additives on lithium-ion mobility in a polymer electrolyte. Tartu, 2003.
42. **Villu Repän.** Low current mode of negative corona. Tartu, 2004.
43. **Алексей Котлов.** Оксианионные диэлектрические кристаллы: зонная структура и электронные возбуждения. Tartu, 2004.
44. **Jaak Talts.** Continuous non-invasive blood pressure measurement: comparative and methodological studies of the differential servo-oscillometric method. Tartu, 2004.
45. **Margus Saal.** Studies of pre-big bang and braneworld cosmology. Tartu, 2004.

46. **Eduard Gerškevitš.** Dose to bone marrow and leukaemia risk in external beam radiotherapy of prostate cancer. Tartu, 2005.
47. **Sergey Shchemelyov.** Sum-frequency generation and multiphoton ionization in xenon under excitation by conical laser beams. Tartu, 2006.
48. **Valter Kiisk.** Optical investigation of metal-oxide thin films. Tartu, 2006.
49. **Jaan Aarik.** Atomic layer deposition of titanium, zirconium and hafnium dioxides: growth mechanisms and properties of thin films. Tartu, 2007.
50. **Astrid Rekker.** Colored-noise-controlled anomalous transport and phase transitions in complex systems. Tartu, 2007.
51. **Andres Punning.** Electromechanical characterization of ionic polymer-metal composite sensing actuators. Tartu, 2007.
52. **Indrek Jõgi.** Conduction mechanisms in thin atomic layer deposited films containing TiO_2. Tartu, 2007.
53. **Aleksei Krasnikov.** Luminescence and defects creation processes in lead tungstate crystals. Tartu, 2007.
54. **Küllike Rägo.** Superconducting properties of MgB_2 in a scenario with intra- and interband pairing channels. Tartu, 2008.
55. **Els Heinsalu.** Normal and anomalously slow diffusion under external fields. Tartu, 2008.
56. **Kuno Kooser.** Soft x-ray induced radiative and nonradiative core-hole decay processes in thin films and solids. Tartu, 2008.
57. **Vadim Boltrushko.** Theory of vibronic transitions with strong nonlinear vibronic interaction in solids. Tartu, 2008.
58. **Andi Hektor.** Neutrino Physics beyond the Standard Model. Tartu, 2008.
59. **Raavo Josepson.** Photoinduced field-assisted electron emission into gases. Tartu, 2008.
60. **Martti Pärs.** Study of spontaneous and photoinduced processes in molecular solids using high-resolution optical spectroscopy. Tartu, 2008.
61. **Kristjan Kannike.** Implications of neutrino masses. Tartu, 2008.
62. **Vigen Issahhanjan.** Hole and interstitial centres in radiation-resistant MgO single crystals. Tartu, 2008.
63. **Veera Krasnenko.** Computational modeling of fluorescent proteins. Tartu, 2008.
64. **Mait Müntel.** Detection of doubly charged higgs boson in the CMS detector. Tartu, 2008.
65. **Kalle Kepler.** Optimisation of patient doses and image quality in diagnostic radiology. Tartu, 2009.
66. **Jüri Raud.** Study of negative glow and positive column regions of capillary HF discharge. Tartu, 2009.
67. **Sven Lange.** Spectroscopic and phase-stabilisation properties of pure and rare-earth ions activated ZrO_2 and HfO_2. Tartu, 2010.
68. **Aarne Kasikov.** Optical characterization of inhomogeneous thin films. Tartu, 2010.

69. **Heli Valtna-Lukner.** Superluminally propagating localized optical pulses. Tartu, 2010.
70. **Artjom Vargunin.** Stochastic and deterministic features of ordering in the systems with a phase transition. Tartu, 2010.
71. **Hannes Liivat.** Probing new physics in e+e− annihilations into heavy particles via spin orientation effects. Tartu, 2010.
72. **Tanel Mullari.** On the second order relativistic deviation equation and its applications. Tartu, 2010.
73. **Aleksandr Lissovski.** Pulsed high-pressure discharge in argon: spectroscopic diagnostics, modeling and development. Tartu, 2010.
74. **Aile Tamm.** Atomic layer deposition of high-permittivity insulators from cyclopentadienyl-based precursors. Tartu, 2010.
75. **Janek Uin.** Electrical separation for generating standard aerosols in a wide particle size range. Tartu, 2011.
76. **Svetlana Ganina.** Hajusandmetega ülesanded kui üks võimalus füüsikaõppe efektiivsuse tõstmiseks. Tartu, 2011
77. **Joel Kuusk.** Measurement of top-of-canopy spectral reflectance of forests for developing vegetation radiative transfer models. Tartu, 2011.
78. **Raul Rammula**. Atomic layer deposition of HfO_2 – nucleation, growth and structure development of thin films. Tartu, 2011.
79. **Сергей Наконечный.** Исследование электронно-дырочных и интерстициал-вакансионных процессов в монокристаллах MgO и LiF методами термоактивационной спектроскопии. Тарту, 2011.
80. **Niina Voropajeva.** Elementary excitations near the boundary of a strongly correlated crystal. Tartu, 2011.
81. **Martin Timusk.** Development and characterization of hybrid electro-optical materials. Tartu, 2012, 106 p.
82. **Merle Lust.** Assessment of dose components to Estonian population. Tartu, 2012, 84 p.
83. **Karl Kruusamäe.** Deformation-dependent electrode impedance of ionic electromechanically active polymers. Tartu, 2012, 128 p.
84. **Liis Rebane.** Measurement of the $W \to \tau\nu$ cross section and a search for a doubly charged Higgs boson decaying to τ-leptons with the CMS detector. Tartu, 2012, 156 p.
85. **Jevgeni Šablonin.** Processes of structural defect creation in pure and doped MgO and NaCl single crystals under condition of low or super high density of electronic excitations. Tartu, 2013, 145 p.
86. **Riho Vendt**. Combined method for establishment and dissemination of the international temperature scale. Tartu, 2013, 108 p.
87. **Peeter Piksarv.** Spatiotemporal characterization of diffractive and non-diffractive light pulses. Tartu, 2013, 156 p.
88. **Anna Šugai.** Creation of structural defects under superhigh-dense irradiation of wide-gap metal oxides. Tartu, 2013, 108 p.

89. **Ivar Kuusik.** Soft X-ray spectroscopy of insulators. Tartu, 2013, 113 p.
90. **Viktor Vabson**. Measurement uncertainty in Estonian Standard Laboratory for Mass. Tartu, 2013, 134 p.